Response to reviewer #1

Thank you for your critical and useful comments on our manuscript. We have addressed the issues you have raised.

Concerning the term "realistic", this may be overstated; in any case, it should not have been stated as an absolute but rather a relative notion, as we do in the introduction ("more realistic"). In the title, we have replaced "realistic" for "improved"; as this is a relative term, and does not have the weight of "realism", ontologically or elsewise.

Particle concentration effect

> While Hayes et al., 2015b (cited in the paper), found strong evidence for a particle concentration effect on Kd values in the Geotraces data sets from the North Atlantic Ocean, that is ignored in the model. The particle concentration has been documented numerous times (not just by Honeyman and Santschi, 1989, cited in Hayes et al., 2015b) for radioisotopes of Th and other elements, and is ascribed to the existence of sorbing and complexing colloidal organic matter in the filter-passing fraction. This then causes linear correlations of the log of the particle-water partition coefficient (K or Kd) vs. the log of the suspended particle concentration, as well as linear correlation of the log of the sorption rate constant vs. the log of the suspended particle concentration. It would gather that this should be pretty straightforward to incorporate that in the model. This would be important, especially if they intend to model boundary scavenging and nepheloid layer scavenging, where particle concentrations would be expected to be higher, and associated Kd values lower.

The authors are aware of the evidence for K_d values to depend on the particle concentration; we should have discussed and considered this more carefully. Indeed, especially where particle concentrations are high, as near the boundaries and in nepheloids, scavenging would be too high if they were included in our model. In the paper, we advise that future versions include those particles, and we now also note that the particle concentration effect

should be considered.

The inverse correlation between log(K_d) and log(particle concentration) strongly relies on the K_d observed for very high particle concentrations. In the model presented here, particle concentrations of the different phases vary by a factor of 10 or so, so the impact on the K_d value is limited and likely within the spread of the values inferred from the data.

Choice of partition coefficients

In our model, instead of making K_d explicitly dependent on the particle concentration, there are actually different particle sizes, albeit the minimal of two. We have tested different K_d values for Th-230 and Pa-231 for a total of six particle types (small and big POC, opal, calcium carbonate and small and big lithogenic particles). Careful thinking is needed to see where more detail must be added. The particle concentration effect is certainly one to think of, but more particle types and size classes may be at least as important, or at least, in our opinion, those should be the next step in model development as the mechanisms are better understood.

We have also constrained the K_d values in terms of internal consistency. For instance, considering that smaller particles have a larger effective surface, the ratio of K_d's between small and big need to be the same for Th and Pa, at least of a given particle type. The choice for the relatively small K_d values (which are close to the range of (Geibert and Usbeck 2004)) is mostly because of the fact that we only have fast-sinking opal and calcium carbonate particles that would export too much Th and Pa if we were to set a higher value. We did not fully realise that this is a misuse of the results of (Geibert and Usbeck 2004); we are more clear about this now. We checked with W. Geibert that the authors *did* clean their samples, as is described in their methods section, giving rise to your criticism (W. Geibert, pers. comm., January 2018).

Other comments

> Also, the nomenclature and units used in this table are non-conventional. At least, it should be mentioned what the unit of

> Kd (Mg/g) in Table 2 is, i.e., 10^6 g water/g particles. It is not obvious as M can be used for 10^3 and for 10^6.

"M" stands for one million (BIPM et al. 2008). We agree that it should be mentioned that it is mass of water per mass of particle, so we will amend this.

> In Table 3, they review the very limited data sets that they used for their model. By doing that, they omit data sets from many other researchers and oceans. For example, the Th and Pa nuclide data from the Gulf of Mexico (Roberts et al., 2009), or the 230Th and 234Th data sets from the North Atlantic by Guo et al. (1995), which also exhibit the common particle concentration effect, could have been used as well.

A wider range of data sources could be very useful, but we chose to only use a couple, typically more recent and larger, data sets. However, we mostly used what we came across, especially from the GEOTRACES programme, and this we deemed sufficient for a basic analysis of this first model. In the future we should see to using more data; any ready compilations of data in a convenient format would be especially handy.

> Table 4 is totally confusing and to some extent, mislabeled, and needs a better caption stating what the numbers in each column signify, and their units.

The unit is percentage for all fields with respect to all particle phases; we make this more clear now. We added a bit of linespace at the right place for an improved interpretation.

> It should therefore be more clearly stated in the manuscript what they are doing with a very limited data set from which they chose their adjustable parameters. Thus, using more realistic values of K, for example, the simulations might be different.

We have tried simulations with different values of K: they give different results indeed. (J. Dutay et al. 2009) and others have presented several sensitivity simulations with different K's. We don't see need to repeat those. We tried to seek a compromise between "realistic simulation" and reported values. We have the impression that reported values of the K values are uncertain, and that our choice of values are still within that uncertainty. This is a somewhat subjective uncertainty in that it is bigger than reported standard deviations,

because values found in the different studies often fall outside their respective internal distributions. From this we took the liberty of choosing convenient values. We have preformed one sensitivity test to investigate its impact on the Pa/Th ratio.

> Another limitation is that only towards the end of the paper is it stated that the large/small particle designation is using a 50 m boundary. It should then also be considered that not everywhere in the ocean do the large particles sink fast, and the small ones slow. For example, Xu et al. (2011) and Hung et al. (2010, 2012) demonstrated through thorium radioisotopic evidence and microscopic analysis of sediment trap particles collected in oligotrophic waters in the Gulf of Mexico and the Pacific Ocean that the fast sinking particle assemblage is mostly composed of smaller than 50m diatom particles. Thus, without considering this detailed data set, the modeling of van Hulten et al. is, to say the least, unrealistic.

We agree that all sinking particles are not necessarily in the > 50 micron size range. This limit is often set as an operational and somewhat arbitrary limit. However, it makes sense to keep a distinction between suspended/slowly sinking particles (defined operationally as > 0.4 micron or so) and large/rapidly sinking particles (Bacon et al. 1985). (Hung, Gong, and Santschi 2012) obtained their conclusions by comparing POC fluxes determined in sediment traps and approaches based on size-fractionated suspended particulate ^{234}Th and POC concentrations. While they question the use of 50 microns to separate small and large particles, they do not question the occurrence of two distinct behaviors. In addition, (Hung, Gong, and Santschi 2012), focused on ^{234}Th in shallow waters. ^{234}Th and ^{230}Th have similar chemical properties, they are usually studied in different environments (shallow waters versus deep waters) so that they interact with different particle types and do no correlate with the same elements/phases in trapped particles (Roy-Barman et al. 2005). Hence, it may be difficult to extend the results of Hung et al. to particles in the deep ocean.

Response to reviewer #2

Thank you for your critical and useful comments on our manuscript. We have addressed the issues you have raised.

Recent model studies

> It is remarkable that within 2017 alone three papers on implementing and applying 231Pa and 230Th isotopes into models have been presented [...] I just want to encourage the authors to get into contact with the modellers working on CESM1.3 and Bern3D and others and may think about starting such an inter-calibration project.

This would be an interesting idea, and such a collaboration could also result in new model improvements. Until now it was better to let each group develop its own strategy to simulate Pa and Th in order to encourage creativity, but now that several approaches have been proposed, it would be interesting to intercompare their results, for instance in the context of the GEOTRACES programme.

> General: It seems like the submission of this manuscript felt into the time range of the publication of the Guo and Liu paper. Although it was under open discussion since April, the authors may have missed it. Anyway, they definitely should incorporate the findings of Guo and Liu. As well they could provide a short summary (maybe as a table) on all of these recent model papers and what is different with their approaches, how particle fields are generated, how circulation, the range of adsorption/desorption coefficients etc.

We did see (Gu and Liu 2017) when it came out as a discussion paper. Now that it has passed peer review, we now note their study. We believe it would be better if a future study would compare the different models in detail, possibly as part of an inter-calibration project; because that would express a more neutral point of view (and there will have been time for reflection).

Other comments

> page 1: title: I'm not sure about using the term "realistic particle dynamics" in the title. It slightly implies that previous studies have applied unrealistic particle dynamics, which might true for a few only. What about "new" or "refined" instead of realistic?

We agree that "realistic" is not the best qualification here. We have replaced this word for "improved", because this is, at least for POC, spot on. Lithogenic particles are *new* in the model, but I would call the particles as a whole, including the changes in POC and calcium carbonate, *improved*.

> p2, l133: I think Siddall07 is based on Bern3D.

You are right; we have fixed this.

> p3,l1: what is much too low? Please give numbers/factors.

We now do this.

> l23-26: these sentences seem redundant from p2 and 1

We have reordered and removed text.

> general: please make sure to introduce all used abbreviations. E.g. table 1: OPA?

Repaired.

> table 1: large or big ? Called "big" before.

We now call the big particles "big", consistent with the mathematical notation.

> Fig1 and 3: I'm very sorry but my copy of the manuscript does not show the whole contents of these figures. According to the caption I miss a considerable part of the concept. I tried on a Windows and Linux system.

The "picture" environment, though part of the Copernicus LaTeX-package apparently gives problems in presenting the resulting PDF on at least some systems. It is not acceptable if people cannot see the full figures, so we have compiled separate PDFs from the figures and added them in the usual way in the document, now using the better suited TikZ package.

> p5, l11: Hauglustaine04 is a model approach. Why not using a satellite based particle flux?

We used a model approach for internal consistency. (Hauglustaine et al. 2004) gives a representation of dust deposition, whereas satellite based particle fluxes still need to be converted to a air–sea dust flux (through modelling). Furthermore, (Hauglustaine et al. 2004) was readily available on the ORCA2 grid, and has been used for multiple studies (which would also give easy inter-comparison between different NEMO-based models using this deposition field). Given the high uncertainties in dust deposition, we decided that (Hauglustaine et al. 2004) would be good enough for our purpose.

> Fig2: why are dust depositions explicitly shown, but not other fluxes? Whats the transfer function between fig 2 and fig 5d

There are no other fluxes because other particles are biogenic and generated by the biogeochemical PISCES. We run simulation imposing flux from Fig. 2 and in the first vertical level of the model, the distribution shown in Fig. 5(d) is obtained for dust when transport is applied. More concisely, running the model with the monthly flux of Fig. 2 and Eqs (1) (lines 83 and 84 of trcsms_lith.F90) and (2) (lines 97—100) results in Fig. 5(d).

> Table 2: I may have missed it, but why are the factors of the partition coefficients between small and big 5 for POC and 10 for lithogenics?

Since the idea is that the effective surface area is much larger for small particles compared to big, this indeed raises the question why it is 10 times much larger for Lith compared to 5 times larger for POC. Kinetics of adsorption is different for the different types of particles, so the ratio of K for big versus small particles can be different as well. We chose the factors 5 and 10 because the gave good results. But is it reasonable? We decided to fix, for a given particle type, a partition coefficient ratio for the different size classes that is the same for both Th and Pa, with the underlying idea that the relative amount of adsorption spots for large versus big should be the same for any metal. Between different particle types, however, we were more lenient, in that we don't assume anything about the surface structure of any particle, thus small versus big could work differently for lithogenic versus organic-carbon particles.

> p9, l14: as mentioned before it might be helpful to give the range

of the reported values.

It is difficult to give a precise range of that, because different methods are involved in the different observational studies. During the early development of the model we have documented a range based on the values given by (Hayes 2015), (Geibert and Usbeck 2004) and several modelling studies. We have presented those in a supplement to the paper. We think it is better to leave a more detailed analysis and discussion to a different study. For the present study, our effort went to the model framework, which is the embedding of the basic Th/Pa model (ProThorP) in NEMO and the passive-tracer component TOP.

> p9, l18: when it comes to particles sizes I consider (Kretschmer et al., 2008) as an appropriate reference.

This is a presentation, but we found their useful paper on the same subject (doi:10.1016/j.gca.2011.09.012). We've added it in the Discussion.

> table 3: here I have a major concern. The model is compared to an arbitrary core top data set. The Oxford data has a global coverage, but the data is quite old and has been measured by alpha- and beta- counting which comprises large uncertanties. I know that there is little new data from the Pacific and the Southern Ocean, but when it comes to the Atlantic or the Arctic Ocean it would be recommendable to compare the model not only to the two Burckel studies. E.g.:(Bradtmiller et al., 2014; Christl et al., 2010; Hall et al., 2006; Hoffmann et al., 2013; Jonkers et al., 2015; Lippold et al., 2016; Luo et al., 2015; Negre et al., 2010; Roberts et al., 2014) (Rutgers van der Loeff et al., 2016; Voigt et al., 2017). In general it is not clear to me, how the goodness of the model versus observations is assessed (e.g. later on page 14). Wouldn't it be helpful to give some statistics?

We think that the data used is sufficient for this study: it has a good global, especially Atlantic, coverage for a first comparison. It would be useful if a new compilation, put together by "data people" for the highest quality and correct interpretation, were to come available. We are using something that is probably okay for a first comparison, and it would take a disproportionate amount of time to include such data at this time. The same is true for the statistics: we do not think it would add much to the visual sediment plots.

The sediment plots are already additional to the core of this model description paper, which was to present the model. In a model evaluation paper, or in a more regular oceanographic study, a statistical analysis and more up-to-date dataset would be much more important.

> p11,fig.4: later in the text we learn that the model gives too high 231Pa/230Th values (e.g. Fig. 8d). But given that the circulation scheme of Fig. 4 is not realistic (too shallow northern overturning) this is not surprising. What parameters are responsible for creating such a shallow overturning, which reminds me rather of a glacial circulation scheme?

Low resolution models, like with the ORCA2 configuration (2°) we use, a shallow overturning is a common issue. At low resolution, models cannot realistically simulatate small-scale features like vertical mixing, which results in a too shallow overturning. We still used these circulation field because they are "the best" we have for the ORCA2 configuration, in the sense that they are used and discussed in many other studies, e.g. (Gehlen et al. 2007,Arsouze et al. (2009),J. Dutay et al. (2009),Aumont et al. (2015)). Probably, it is best if models of higher resolution are considered, but that is expensive in combination with a full biogeochemical model and we considered this from the beginning out of the scope of this study.

> p11, l 10: ". . .has a strong overturning. . ." relative to what?

Relative to some estimates. Even though it is not precisely known what the transport in the lower cell is, the model quite certainly overestimates it (citation has been added to the paper). The reasoning starts with that we are using a model with a relatively low resolution, which typically have a too shallow (upper) overturning (as the one we use does). Because of this, there is a much larger depth range in which the lower overturning cell can transport AABW northward, resulting, at least in our case, in an overestimated flux.

> Fig. 5: What are the observations shown here based on? Please give references in the caption. I'm sure there are more observations available than shown here. The color codes seem to be scaled by arbitrarily increasing numbers. However, more important, the model generates impressively realistic particle fields, but what about this high production region off Argentina?

Information on particle sources included in caption, and more information

in-text. We are not aware of observations of particle concentrations that could improve our coverage. (Lam, Doney, and Bishop 2011) collected (consistent) data from previous studies, and should cover all data up to 2011. Since then the GEOTRACES programme has new data at the GA03 transect, but we don't know of other data. For instance, to our knowledge there are no surface concentrations of biogenic particles available in the Argentine Basin. The Argentine Basins is a specific region of high productivity with a large continental margin; of course, it would be nice if we could validate our model to concentration measurements.

> p12, l 9-11: I don't understand this sentence.

We have rephrased part of this paragraph for clarity.

> Fig. 8: I appreciate the overall good agreement with observations. But, as mentioned before, the deep could be much better with a realistic overturning scheme.

Yes.

> Fig. 10: caption: "Concentrations.." of what? Please provide units.

Units are added now.

> Table 4/p 16, l 3-4: Maybe more explanation needed here on the difference between "stock" and "particle flx". What creates the huge difference for both between bSiO2 and Litho.?

Only for POC and Litho do we have slowly sinking particles on which much of the stock is stuck, whereas the big affinity of Pa to bSiO mostly results in a strong export (and similarly for Th on CaCO3). We have added this to the text.

> Fig. 11 and Fig. 13: Please use same scale for both plots (0.0 to 0.30 at max. Higher values are unrealistic). As mentioned before, please use an up-to-date data base for the Atlantic. Further it would be helpful to show the Atlantic model and observations in a 231Pa/230Th vs. depth plot like done by (Gherardi et al., 2009) (their figure 5).

We have set the same colour scales with the maximum at 0.30 (and with a "Δ" for higher, unrealistic values).

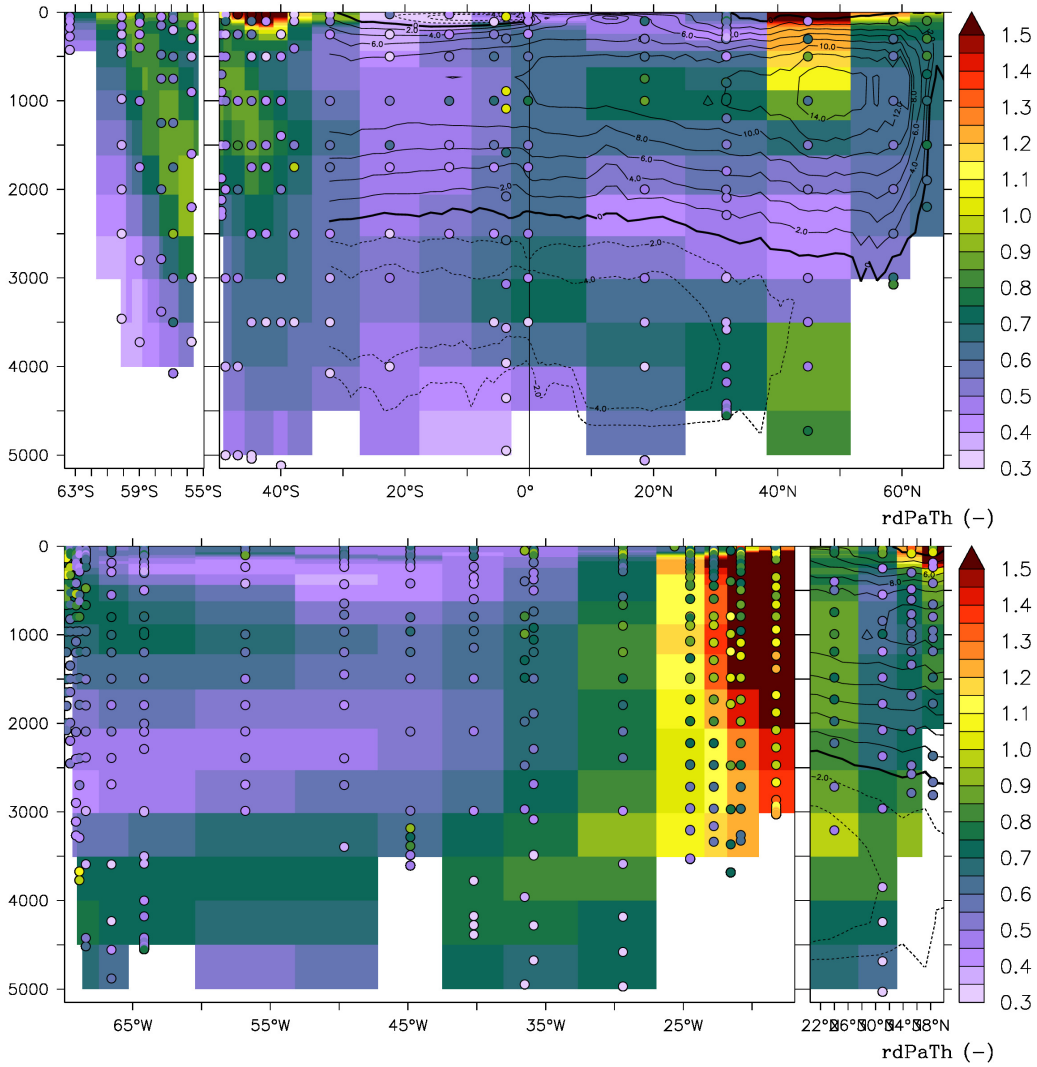

In these figures we show the dissolved Pa-231/Th-230 concentration in the seawater at the meridional GA02 (and Drake Passage), and the North Atlantic GA03 transects. Several of the patterns in the observations are recognisable in the model, but there are discrepancies as well. As of yet we don't have any interpretations of this that would give more insight in the model and ocean processes than what we got from the other figures. We could perhaps add them to an electronic supplement?

> p20: […] I want to suggest that the data mentioned in the "second line 7" (hydrothermal) could be indicated by different symbols

in Fig. 12. This would enable to see where the model fails and where not.

We have indicated the gridbox corresponding with hydrothermal now with a different symbol. More importantly, we found an issue with how we processed the GA03 data for the statistics. Now doing it properly, results in a much better model—data correlation at the GA03 transect than we thought before.

chapter 6.1: the "weaker" affinity of Pa to opal is a very interesting finding. In order to strengthen this point it could be helpful to provide an overview of all the values proposed by the different studies, in particular by describing if it was a lab-experiment, in situ observation (where) or the best fit for the model.

We agree that this would be useful, but it is out of the scope of this study. The apparently weaker affinity of Pa to opal was meant as an additional illustration of the model; we do realise that it does warrant a more extensive study, and we hope that our illustration does not stop anyone from doing this in a rigorous way.

Response to reviewer #3

Thank you for your critical and useful comments on our manuscript. We have addressed the issues you have raised.

Scientific Quality

1. I do not believe that one of the central assumptions is justified. You assume that the absorption and desorption rates are much faster than the settling of the absorbed phases. This is marginally true for small particles sinking at 2 m/day, but is not at all true for particles sinking at 50 m/day. […]

The authors must either justify in detail why the assumption is valid (and thus explain why my analysis is in error) or include the absorption/desorption process.

ProThorP's aim is to scavenge and vertically transport Pa-231 and Th-230 while ocean water masses are flowing around to describe mainly (1) the amount of dissolved Pa and Th left in the water column and (2) the Pa/Th ratio accumulated in the sediments. It is clear that the equilibrium between dissolved and large particles is convenient for computing but not necessarily realistic in terms of processes at the scale of a single large particle. One idea, which is not in the equation and that might not be verified is that no "true" (chemically speaking) equilibrium between the dissolved phase and big particles exists, but that aggregation of small particles (probably through grazing) ensures the transert of Pa and Th from the solution to the large particles (Bacon and anderson, 1985). But this is not the real issue. The issue is to describe Pa–Th fluxes at the water column scale. Hence, when small and large particles are present (litho, POC), the Kd for the big particles is reduced compared to small particles so that large particles do not completely deplete the water column in Th and Pa. Similarly when only large particles are present (e.g., small carbonate, which is certainly not realistic either), the Kd(Th) is reduced compared to the values determined experimentally by Hayes et al. to ensure realistic fluxes.

This "fast equilibrium" hypothesis is certainly the reason for the very low dissolved ^{230}Th concentration modelled in the surface water (Fig. 9). This is equally due to small and big particles and not of great importance because we are not particularly interested in the surface water distribution or Pa and Th.

2. Why did you chose 20% small and 80% large for your lithogenic particles?

We tried 20 and 80% partitioning of dust into the lithogenic ocean particles, and this happened to work well. As explained in the manuscript, dust particles must aggregate in the upper ocean to get anywhere close to the concentration of large lithogenic particles observed in the ocean. We quickly settled on the 20/80%, because tuning would overestimate the dust source where we are missing resuspended particle sources. Further refinement should therefore be developed together with those other sources.

3. pg 16, last line : "These discrepancies …. arise from the different speeds for each type of particle" But don't all big particles sink at the same rate? I think you could make this more clear but adding columns to Table 4: small Litho, big Litho, total Litho etc.

We think that would be too much information. We have clarified the interpretation in the text; we hope that it is more clear now.

4. pg 22 Lines 10-20: also consider including Luo et al (2010) in this discussion as their simple model allows one to see the impact more easily

Yes, we now refer to them in this context.

Scientific Reproducibility

1. How long was the NEMO-OPA model run? Was a single year of forcing used repeatedly? If so, what year? If not, what years of forcing were used?

The simulation was produced with climatological conditions. Thus, there is no interannual variability in the forcing dataset. The model has been run for 200 years and the last year has been selected. Since the model was forced by climatological conditions, there is no interannual variability in the ocean dynamics that is simulated except for the internal variability which at 2° resolution is negligible almost everywhere except perhaps in the equatorial regions. Thus, choosing whatever year is valid.

2. Was an ice model included?

Yes, this was a simulation with NEMO-LIM.

3. Please include the fourth order equation for CaCO 3 dissolution.

Done.

4. I don't think you actually code equation (5). If I'm correct, please give the equations you actually code.

We have not coded it exactly like this, but there will always be a translation step between the mathematical model and the implementation. The production (β) and decay ($-\lambda A$) of the radioisotopes are defined in trcsms_protac.F90 and are straightforwardly transcribed from the equations. The sinking term ($w\mathrm{d}A/\mathrm{d}z$) is in p4zsink.F90, and has some subtleties, but does implement this term. Finally, the circulation including eddy-induced velocity (in the full derivative) as well as the diffusion terms ($\mathcal{A}$ for horizontal

and $\mathcal{B}$ for vertical) are in OPA, and one will get the right routines through a full check-out of the NEMO repository. Since we are running PISCES and the added passive tracers off-line with respect to OPA, should we better not write out the dynamical terms. We could then just mention again that the tracers are advected by an off-line circulation field (same for eqn 2). Please, advice.

5. Under Simulations, first sentence "The model" please specify that this is the PISCES+tracer model.

Done.

6. Please include a run table, showing your physical run, your spin-up and your two analyzed runs.

We have not included a table, because there is only one sensitivity simulation, which is not central to the paper. There is one base simulation of Pa-231 and Th-230, and the dynamics is a forcing that is evaluated and used in multiple studies before.

7. Link biogenic silica and opal, in case your readers don't understand you are using them interchangeably.

Instead of linking them, we decided to replace the couple of occurrences of "opal" with "biogenic silica".

8. Where does one get the new scavenging model?

Near the end of the paper there is a section on code availability. There is the link to the code (https://zenodo.org/record/1009065). This archive contains updated PISCES routines, lithogenic particles and the Th-230 and Pa-231 code (including scavenging).

Presentation Quality

1. pg 1, l 19 "and the carbon"
2. Fig 1 "triple"
3. pg 5, l 7 "corresponding to"
4. pg 5, l 14 "(e.g. Van Hulten et al, 2013)"
5. pg 9, l 22 "a large number of measurements"
6. pg 9, l 23 "on this transect"

7. Table 3: over run on second last line.
8. pg 11, l 5 drop “thereof”
9. pg 11, l 11 “water sinks down”
10. pg 11, l 12 “Antarctic”
11. pg 12, l 10 “whereas we only have small particle data for the Atlantic Ocean”
12. pg 14, l 6 drop “as well”
13. pg 15, l 14 “Globally in the model,”
14. pg 16, l 12 “discrepancies”
15. pg 19, l3 or 18 depending how you count! “POC accounts for only”

Thank you for these corrections! We applied the changes.

Arsouze, T., J.-C. Dutay, F. Lacan, and C. Jeandel. 2009. “Reconstructing the Nd oceanic cycle using a coupled dynamical–biogeochemical model.” *Biogeosci.* 6 (12). European Geosciences Union: 2829–46. doi:10.5194/bg-6-2829-2009.

Aumont, O., C. Ethé, A. Tagliabue, L. Bopp, and M. Gehlen. 2015. “PISCES-V2: An Ocean Biogeochemical Model for Carbon and Ecosystem Studies.” *Geosci. Model Dev.* 8 (8): 2465–2513. doi:10.5194/gmd-8-2465-2015.

Bacon, Michael P., Chih-An Huh, Alan P. Fleer, and Werner G. Deuser. 1985. “Seasonality in the Flux of Natural Radionuclides and Plutonium in the Deep Sargasso Sea.” *Deep-Sea Res. Pt A* 32 (3): 273–86. doi:10.1016/0198-0149(85)90079-2.

BIPM, IEC, ILAC IFCC, IUPAP IUPAC, and OIML ISO. 2008. “The International Vocabulary of Metrology: Basic and General Concepts and Associated Terms (VIM), 3rd Edn. JCGM 200: 2012.”

Dutay, J.C., F. Lacan, M. Roy-Barman, and L. Bopp. 2009. “Influence of particle size and type on ^{231}Pa and ^{230}Th simulation with a global coupled biogeochemical-ocean general circulation model: A first approach.” *Geochem. Geophy. Geosy.* 10 (1). American Geophysical Union: Q01011. doi:10.1029/2008GC002291.

Gehlen, M., R. Gangstø, B. Schneider, L. Bopp, O. Aumont, and C. Ethé. 2007. “The Fate of Pelagic $CaCO_3$ Production in a High CO_2 Ocean: A

Model Study." *Biogeosci.* 4 (4): 505–19. doi:10.5194/bg-4-505-2007.

Geibert, Walter, and Regina Usbeck. 2004. "Adsorption of Thorium and Protactinium onto Different Particle Types: Experimental Findings." *Geochim. Cosmochim. Ac.* 68 (7). Elsevier: 1489–1501. doi:10.1016/j.gca.2003.10.011.

Gu, S., and Z. Liu. 2017. "^{231}Pa and ^{230}Th in the Ocean Model of the Community Earth System Model (CESM1.3)." *Geosci. Model Dev.* 10 (12): 4723–42. doi:10.5194/gmd-10-4723-2017.

Hauglustaine, D.A., F. Hourdin, L. Jourdain, M.-A. Filiberti, S. Walters, J.-F. Lamarque, and E.A. Holland. 2004. "Interactive Chemistry in the Laboratoire de Météorologie Dynamique General Circulation Model: Description and Background Tropospheric Chemistry Evaluation." *J. Geophys. Res.: Atmospheres* 109 (D4): D04314. doi:10.1029/2003JD003957.

Hayes, Robert F. AND Fleisher, Christopher T. AND Anderson. 2015. "Intensity of Th and Pa Scavenging Partitioned by Particle Chemistry in the North Atlantic Ocean." *Mar. Chem.* 170. Elsevier: 49–60. doi:10.1016/j.marchem.2015.01.006.

Hung, Chin-Chang, Gwo-Ching Gong, and Peter H. Santschi. 2012. "^{234}Th in Different Size Classes of Sediment Trap Collected Particles from the Northwestern Pacific Ocean." *Geochim. Cosmochim. Ac.* 91: 60–74. doi:10.1016/j.gca.2012.05.017.

Lam, Phoebe J., Scott C. Doney, and James K. B. Bishop. 2011. "The Dynamic Ocean Biological Pump: Insights from a Global Compilation of Particulate Organic Carbon, $CaCO_3$, and Opal Concentration Profiles from the Mesopelagic." *Global Biogeochem. Cy.* 25 (3): GB3009. doi:10.1029/2010GB003868.

Roy-Barman, M., C. Jeandel, M. Souhaut, M. Rutgers van der Loeff, I. Voege, N. Leblond, and R. Freydier. 2005. "The Influence of Particle Composition on Thorium Scavenging in the NE Atlantic Ocean (POMME Experiment)." *Earth Planet. Sc. Lett.* 240 (3). Elsevier: 681–93. doi:10.1016/j.epsl.2005.09.059.

List of changes in the manuscript

- changed title ("realistic" -> "improved");
- improved figures 1 and 3 (sharp, visible and consistent);
- added information on calcium carbonate parameterisation (Section 2.2);
- improved on the description of the off-line physics (e.g. p. 9);
- moved the figure of the overturning to supplement;
- added information on our error (rightly pointed out by a reviewer) on interpreting and using data from Geibert and Usbeck (2004) (p. 10);
- improved (or attempted at least) Table 4 (p. 18) and its description (text p. 19);
- made the cut-off of 51 m diameter and correspondence with particle sizes bit more clear;
- because of an error we made in the statistics of the data–model comparison at the GA03, we included the newly calculated correlation coefficient and in the supplement the correct scatter plot of GA03;
- included references to relevant studies that we have overlooked before (or were not yet final publications);
- minor changes marked up in green;
- included supplementary document with figures and tables and statistics;
- PANGAEA publication of model data is in progress (open issue), and should be added at final publication; right now, reviewers may access it through `http://klimato.org/pub/prothorp_output.tar.gz` if they wish so.

A global scavenging and circulation ocean model of thorium-230 and protactinium-231 with improved particle dynamics (NEMO–ProThorP 0.1)

Marco van Hulten[1,2], Jean-Claude Dutay[1], and Matthieu Roy-Barman[1]

[1]Laboratoire des Sciences du Climat et de l'Environnement, IPSL, CEA–Orme des Merisiers, 91191 Gif-sur-Yvette, France
[2]Geophysical Institute, University of Bergen, Bergen, Norway

Correspondence to: M. M. P. van Hulten <Marco.Hulten@uib.no>

Pre- and postprints may be found at arXiv:1708.04157.

Abstract. In this paper, we set forth a 3-D ocean model of the radioactive trace isotopes $^{230}\mathrm{Th}$ and $^{231}\mathrm{Pa}$. The interest arises from the fact that these isotopes are extensively used for investigating particle transport in the ocean and reconstructing past ocean circulation. The tracers are reversibly scavenged by biogenic and lithogenic particles.

Our simulations of $^{230}\mathrm{Th}$ and $^{231}\mathrm{Pa}$ are based on the NEMO–PISCES ocean biogeochemistry general circulation model, which includes biogenic particles, namely small and big particulate organic carbon, calcium carbonate and biogenic silica. Small and big lithogenic particles from dust deposition are included in our model as well. Their distributions generally compare well with the small and big lithogenic particle concentrations from recent observations from the GEOTRACES programme, except for boundary nepheloid layers for which, as up to today, there are no non-trivial, prognostic models available on a global scale. Our simulations reproduce $^{230}\mathrm{Th}$ and $^{231}\mathrm{Pa}$ dissolved concentrations: they compare well with recent GEOTRACES observations in many parts of the ocean. Particulate $^{230}\mathrm{Th}$ and $^{231}\mathrm{Pa}$ concentrations are significantly improved compared to previous studies, but they are still too low because of missing particles from nepheloid layers. Our simulation reproduces the main characteristics of the $^{231}\mathrm{Pa}/^{230}\mathrm{Th}$ ratio observed in the sediments, and supports a moderate affinity of $^{231}\mathrm{Pa}$ to biogenic silica as suggested by recent observations, relative to $^{230}\mathrm{Th}$.

Future model development may further improve understanding, especially when this will include a more complete representation of all particles, including different size classes, manganese hydroxides and nepheloid layers. This can be done based on our model, as its source code is readily available.

1 Introduction

Oceanic circulation and the carbon cycle play a major role in the regulation of the past and present climate. Heat and carbon dioxide in the atmosphere tend to equilibrate with the ocean surface, and are transported down into the deep ocean through the Meridional Overturning Circulation (MOC). Biogeochemical cycling also generates organic carbon that transfers into the

deep ocean through particle sinking. Because of this, the strength of the MOC and particle removal participate actively in the regulation of the climate on the Earth.

Trace elements are also affected by these mechanisms, and represent useful tools to provide constraints on these processes. The GEOTRACES programme has generated a unique, large data set that can now be used to better understand biogeochemical oceanic processes. Modelling quantifies and provides more information on the processes that control the oceanic distribution of these new observations. In present day climate, it is difficult to measure the MOC strength, and for past climate there are no measurements available at all. Isotopes and trace elements from sediment cores are used as proxies to infer past ocean circulation. Several examples include carbon isotopes (Broecker et al., 1988), the cadmium/calcium ratio (Rosenthal et al., 1997), the ratio between protactinium-231 and thorium-230 ($^{231}\mathrm{Pa}/^{230}\mathrm{Th}$) (Böhm et al., 2015), and the neodymium isotope ratio $^{143}\mathrm{Nd}/^{144}\mathrm{Nd}$ (Piotrowski et al., 2005). These proxies are affected by dynamical and biogeochemical processes. Including these proxies in a climate model is a way to better understand the climatic signal they register.

We will focus on $^{230}\mathrm{Th}$ and $^{231}\mathrm{Pa}$, because these isotopes are well documented by the international GEOTRACES programme, and they are particularly suitable to study the transfer of particulate matter since the isotopes' source in the ocean is perfectly known: radioactive decay of uranium isotopes. Others have modelled $^{143}\mathrm{Nd}$ and $^{144}\mathrm{Nd}$ (Arsouze et al., 2008, 2009; Ayache et al., 2016), $^{13}\mathrm{C}$ (Tagliabue et al., 2009) and $^{14}\mathrm{C}$ (Mouchet, 2013). The ratio $^{230}\mathrm{Th}$ and $^{231}\mathrm{Pa}$ is used as a proxy for past ocean conditions, but this signal is potentially affected by both circulation and biogeochemical changes. Therefore, a correct understanding of the scavenging and the underlying particle dynamics is essential in order to better simulate these tracers (Dutay et al., 2015).

Protactinium-231 and thorium-230 are produced in the ocean by the α-decay of uranium-235 and uranium-234, respectively. Because the activity of uranium is approximately uniform in the ocean, $^{231}\mathrm{Pa}$ and $^{230}\mathrm{Th}$ are produced at a relatively constant rate ($\beta_{\mathrm{Pa}} = 2.33 \times 10^{-3}\ \mathrm{dpm\,m^{-3}\,a^{-1}}$ and $\beta_{\mathrm{Th}} = 2.52 \times 10^{-2}\ \mathrm{dpm\,m^{-3}\,a^{-1}}$, dpm = *disintegrations per minute*) (Henderson and Anderson, 2003). They are both scavenged rapidly by the many particles that reside in the ocean and settle towards the seafloor. $^{231}\mathrm{Pa}$ is less sensitive to particle scavenging than $^{230}\mathrm{Th}$, which is reflected in the longer residence time of $^{231}\mathrm{Pa}$ (80–200 yr) compared to that of $^{230}\mathrm{Th}$ (20–40 yr) (Yu et al., 1996). $^{231}\mathrm{Pa}$ and $^{230}\mathrm{Th}$ are radioactive, decaying to radium isotopes and having a half-life of 32.76 kyr and 75.40 kyr, respectively. Each combination of particle–radionuclide adsorption has a different reactivity. There are additional complications such as the typically larger surface of smaller particles where more radionuclides can adsorb onto and the decrease of adsorption rate when particle concentrations become very high (Honeyman et al., 1988; Honeyman and Santschi, 1988). The vertical distributions of natural radionuclides, such as $^{230}\mathrm{Th}$ and $^{231}\mathrm{Pa}$, are hence sensitive to the distribution and mixture of particles. As a consequence of the different particle reactivities of $^{230}\mathrm{Th}$ and $^{231}\mathrm{Pa}$, $\left[^{231}\mathrm{Pa}\right]_D/\left[^{230}\mathrm{Th}\right]_D$ deviates from the production activity ratio of 0.093 (Anderson et al., 1983; Anderson, 2003; Rutgers van der Loeff et al., 2016).

As both particle dynamics and circulation of the ocean affect $^{230}\mathrm{Th}$ and $^{231}\mathrm{Pa}$, numerical biogeochemical general circulation models are used to study the relative contribution of these mechanisms. The isotopes have been simulated in models of intermediate complexity, for instance by Henderson et al. (1999) (LSG-OGCM), Marchal et al. (2000) (EMIC 2.5D), Heinze et al. (2006) (HAMOCC) and Luo et al. (2010). More complex ocean general circulation models models have also been used

to simulate these tracers Dutay et al. (2009) (NEMO–PISCES), Siddall et al. (2007); Rempfer et al. (2017) (Bern3D) and Gu and Liu (2017) (CESM). Dutay et al. (2009) demonstrated that the particle concentration simulated by the PISCES model in the deep ocean was a factor of 2 in the mesopelagic zone to 50 in the deepest ocean too low. This lead to overestimated radionuclide concentrations in the deep ocean. Therefore, it is crucial to improve the representation of the particles (Dutay et al., 2009). Rempfer et al. (2017) showed that taking into account additional sinks at the seafloor and at the ocean margins yields an improved agreement with observations, especially for the dissolved phases of $^{230}\mathrm{Th}$ and $^{231}\mathrm{Pa}$. Particulate ratios improved to a lesser extent; the authors have not presented evaluation of their simulated particulate concentrations. Gu and Liu (2017) had similar goals as this study.

In this study, we try to improve on previous studies that simulate the distribution of $^{230}\mathrm{Th}$ and $^{231}\mathrm{Pa}$. Our approach is to improve the mechanistic description of the particle and radionuclide cycling, as well as on the side of system design and reusability of the model. We evaluate how well the model fits with observations, but tuning is not one of our main goals. Just like Dutay et al. (2009), we use the NEMO–OPA (Nucleus for European Modelling of the Ocean – Océan PAralelisé) ocean general circulation model (Madec and the NEMO team, 2016) and the PISCES biogeochemical model (Aumont et al., 2015). Aumont et al. (2017) showed that dissolution rates of Particulate Organic Carbon (POC) in PISCES were overestimated, and they improved on this by introducing a spectrum of different labilities. This improved the simulation of both small and big POC significantly, so we use this same model for our simulations. There are several improvements since Dutay et al. (2009), namely the new model

- includes lithogenic particles from dust deposition;
- improved the biogeochemistry, affecting the biogenic particle distributions (Aumont et al., 2015, 2017);
- includes three different phases per nuclide (dissolved, and adsorbed onto big (and small) particles), whereas Dutay et al. (2009) include only a single compartment (total concentration) for each nuclide from which they calculated the respective phases based on chemical equilibrium;
- is more precise/explicit on the mathematical formalism;
- is written in Fortran 95 instead of Fortran 77, making the extension of its use to other modern Fortran models easier;
- is part of a modern model framework, NEMO–TOP, facilitating its use with other models in this framework.

The main objective of this paper is to improve on the simulation of $^{230}\mathrm{Th}$ and $^{231}\mathrm{Pa}$ (the dissolved and two particulate size classes of particles for both nuclides), based on an improved modelling of small and big particles.

New observations are available from the GEOTRACES programme. Especially the North Atlantic GA03 transects will be used for model validation; because on this transect not only dissolved $^{230}\mathrm{Th}$ and $^{231}\mathrm{Pa}$ have been measured (Hayes et al., 2015b), but also their adsorbed forms (Hayes et al., 2015b) and biogenic and lithogenic particle concentrations in two size classes (Lam et al., 2015).

model component	improvements or relevant properties	timestep
circulation (OPA)	prescribed forcing (off-line physics) (e.g. used by Arsouze et al., 2009)	6.0 h
biogenic particles	prognostically integrated by PISCES (Aumont et al., 2015)	1.5 h
– POC	two size classes settling with $w_s = 2\,\mathrm{m\,d^{-1}}$ and $w_b = 50\,\mathrm{m\,d^{-1}}$; variable reactivity (Aumont et al., 2017)	
– $CaCO_3$	one size class settling with $w_b = 50\,\mathrm{m\,d^{-1}}$; higher order dissolution (e.g. Subhas et al., 2015)	
– $bSiO_2$	one size class settling with $w_b = 50\,\mathrm{m\,d^{-1}}$; no changes	
lithogenic particles	based on forcing of dust deposition; two size classes settling with $w_s = 2\,\mathrm{m\,d^{-1}}$ and $w_b = 50\,\mathrm{m\,d^{-1}}$	1.5 h
radionuclide model	six prognostic tracers (dissolved, small and big adsorbed; $^{231}\mathrm{Pa}$ and $^{230}\mathrm{Th}$)	6.0 h

Table 1. Model components and properties essential for the radionuclide model. OPA stands for Océan PAralalisé.

2 Model description

In order to simulate the biogenic particle dynamics and its interaction with the $^{230}\mathrm{Th}$ and $^{231}\mathrm{Pa}$ trace isotopes, we use the biogeochemical circulation model NEMO–PISCES (Madec, 2008; Aumont et al., 2015). This model has been employed for many other studies concerning trace metals, as well as large-scale ocean biogeochemistry (e.g. Gehlen et al., 2007; Arsouze et al., 2009; Dutay et al., 2009; Tagliabue et al., 2010; Van Hulten et al., 2013, 2014, 2017b). We force PISCES by a climatological year of circulation fields (including turbulent diffusion) that was obtained from the dynamical component of the *Nucleus for European Modelling of the Ocean* (NEMO). Table 1 gives an overview of this and other components of the model and their relevant properties.

All model fields are defined on the ORCA2 discrete coordinate system, an irregular grid covering the whole world ocean with a nominal resolution of $2^\circ \times 2^\circ$, with an increased resolution in the meridional direction near the equator and Antarctica, and in both horizontal directions in the Mediterranean, Red, Black and Caspian Seas. On the Northern Hemisphere, it has two coordinate singularities, one in Canada and the other in Russia, such that both singularities fall outside the computational domain. The vertical resolution of the ORCA2 grid is 10 m in the upper 100 m, increasing downwards to 500 m, such that there are 30 layers in total and the ocean has a maximum depth of 5000 m (Madec and Imbard, 1996; Murray, 1996). The timestep of the model is 6 h for the dynamics and the radionuclides, and 1.5 h for the biogeochemistry (PISCES) and the lithogenic particles. When necessary, sub-timestepping is done for all sinking components in the model.

2.1 Circulation

The circulation was obtained by forcing NEMO in the ORCA2 configuration with climatological air-sea boundary conditions, consisting of heat, fresh water and momentum fluxes that were derived from bulk formulae. They are functions of wind, sea surface temperature, air temperature, air humidity and evaporation minus precipitation. For the tropics, daily wind stress was used, which was based on European Remote Sensing (ERS) satellite data, and for the polar regions, NCEP/NCAR re-analysis data (Kalnay et al., 1996; Kistler et al., 2001). Surface salinity was restored with a timescale of 60 days towards the seasonal

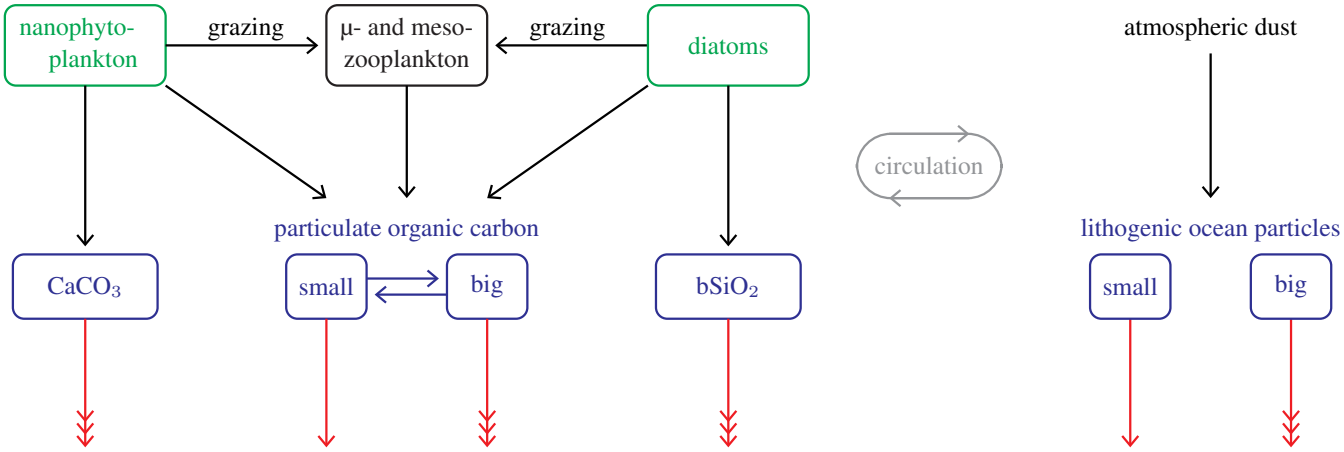

Figure 1. Conceptual model of particle dynamics, on which the numerical model is based. Nanophytoplankton and diatoms (in green) take up nutrients and CO_2, which are released again from respiration and remineralisation of $bSiO_2$, POC, DOM and lithogenic particles. The nutrients are not represented in the figure, because only particles impact ^{231}Pa and ^{230}Th. Zooplankton are denoted by the black box. All sinking particles are denoted by blue boxes. Effectively, this figure comprises the internal cycling of PISCES, minus details that are not of interest here, plus the lithogenic dust model. DOM stands for Dissolved Organic Carbon, sPOM and bPOM stand for small and big Particulate Organic Matter which are both subject to the differential lability scheme (Aumont et al., 2017), and $bSiO_2$ stands for biogenic silica. Sinking is denoted by the red arrows; triple arrows means fast, normal arrows slow.

Polar Science Center Hydrographic Climatology (PHC) dataset to avoid model drift (Timmermann et al., 2005). The last year of this 200-year simulation is used as our one-year climatology with a resolution of five days of the dynamics.

2.2 Particle dynamics

This version of PISCES includes two size classes of POC, both with differential remineralisation rates (Aumont et al., 2017), one class of biogenic silica ($bSiO_2$) and one class of calcium carbonate ($CaCO_3$). In the model, particles sink down with two velocities: $w_s = 2\,\mathrm{m\,d^{-1}}$ and $w_b = 50\,\mathrm{m\,d^{-1}}$. As we need to compare with observations, these can be taken to correspond with "small" particles ($\varnothing \leq 51\,\mu\mathrm{m}$) and "big" particles ($\varnothing > 51\,\mu\mathrm{m}$) (Fig. 1).

The dissolution equation for calcium carbonate is given by

$$\frac{\mathrm{d}[\mathrm{CaCO_3}]}{\mathrm{d}t} = -R[\mathrm{CaCO_3}]\,, \tag{1}$$

where the rate variable (constant in t) for calcite dissolution is

$$R = k \cdot (1-\Omega)^n\,, \tag{2}$$

where k and n are two somewhat restricted, though tunable, parameters that signify a dissolution rate constant and a reaction rate order, respectively. The calcite saturation state is given by:

$$\Omega = \frac{[\mathrm{Ca}^{2+}][\mathrm{CO}_3^{2-}]}{K'_{sp}}\,, \tag{3}$$

where K'_{sp} is the product of the saturation concentrations of calcium and carbonate. This can be approximated by:

$$\Omega \approx \frac{[\mathrm{CO}_3^{2-}]}{[\mathrm{CO}_3^{2-}]_{\mathrm{sat}}}\,, \tag{4}$$

because relative variations in $[\mathrm{Ca}^{2+}]$ are small. For $\mathrm{CaCO_3}$ we changed the standard first-order dissolution kinetics parameterisation to a fourth-order dissolution, based on evidence of Keir (1980) and subsequent studies. For our simulation we used a calcite dissolution rate constant of $k = 2.5\ \mathrm{mo}^{-1}$ and a dissolution order of $n = 3.9$ (Subhas et al., 2015).

In addition to biogenic particles, we introduced lithogenic dust particles in the model. The yearly average dust flux is derived from Hauglustaine et al. (2004) and is presented in Fig. 2. It is used by the model as the input of lithogenic ocean particles as well as for nutrient supply in PISCES. This dust deposition field has been tested in biogeochemical studies with this configuration of NEMO (e.g. Van Hulten et al., 2013).

Small and big lithogenic particles are added to the upper layer of the ocean according to:

$$\frac{\partial P^{\mathrm{Litho}}}{\partial t}\Big|_{\mathrm{surface}} = \frac{f}{\Delta z_1} \cdot \Phi_{\mathrm{dust}}\,, \tag{5}$$

where P^{Litho} is the small (big) lithogenic particle concentration, f is the fraction of the dust that gets partitioned into the small (big) lithogenic particles in the ocean, $\Delta z_1 = 10\ \mathrm{m}$ is the thickness of the upper model layer, and Φ_{dust} is the dust flux.

Our model has two size classes for lithogenic particles, so this equation is applied for two different concentrations P^{Litho} and respective fractions f. We set the small lithogenic dust flux fraction to 20 % and the big one to 80 %. Once partitioned in the ocean, the lithogenic particles sink down, changing their concentrations throughout the ocean according to

$$\frac{\mathrm{d}P^{\mathrm{Litho}}}{\mathrm{d}t} = -w \cdot \frac{\partial P^{\mathrm{Litho}}}{\partial z} + \left(\mathcal{A}\nabla_h^2 + \mathcal{B}\frac{\partial^2}{\partial z^2}\right) P^{\mathrm{Litho}}\,, \tag{6}$$

where w is the settling velocity, set to the constant $2\ \mathrm{m\,d}^{-1}$ for the small lithogenic particles and to $50\ \mathrm{m\,d}^{-1}$ for the big particles. The depth, z, is positive upwards, ∇_h is the horizontal divergence, and $\mathcal{A}$ and $\mathcal{B}$ are respectively the horizontal and vertical eddy diffusivity coefficients. The material derivative includes a term for eddy-induced velocity (Gent and McWilliams, 1990; Gent et al., 1995). Equation (6) is identical to the settling of small and big POC (Aumont et al., 2015). Of course, there are also biological and chemical sources and sinks for POC. However, for lithogenic particles there are no such sources or sinks because the only source in our model is dust deposition and we assume the lithogenic particles are refractory. The lithogenic particles are removed from the model domain when arriving at the seafloor, which means that they are buried in the sediment.

2.3 Radionuclides

Thorium-230 and protactinium-231 are produced throughout the ocean from the decay of $^{234}\mathrm{U}$ and $^{235}\mathrm{U}$, respectively. Because of long residence times of over 200 kyr, these uranium isotopes are approximately homogeneously distributed throughout the

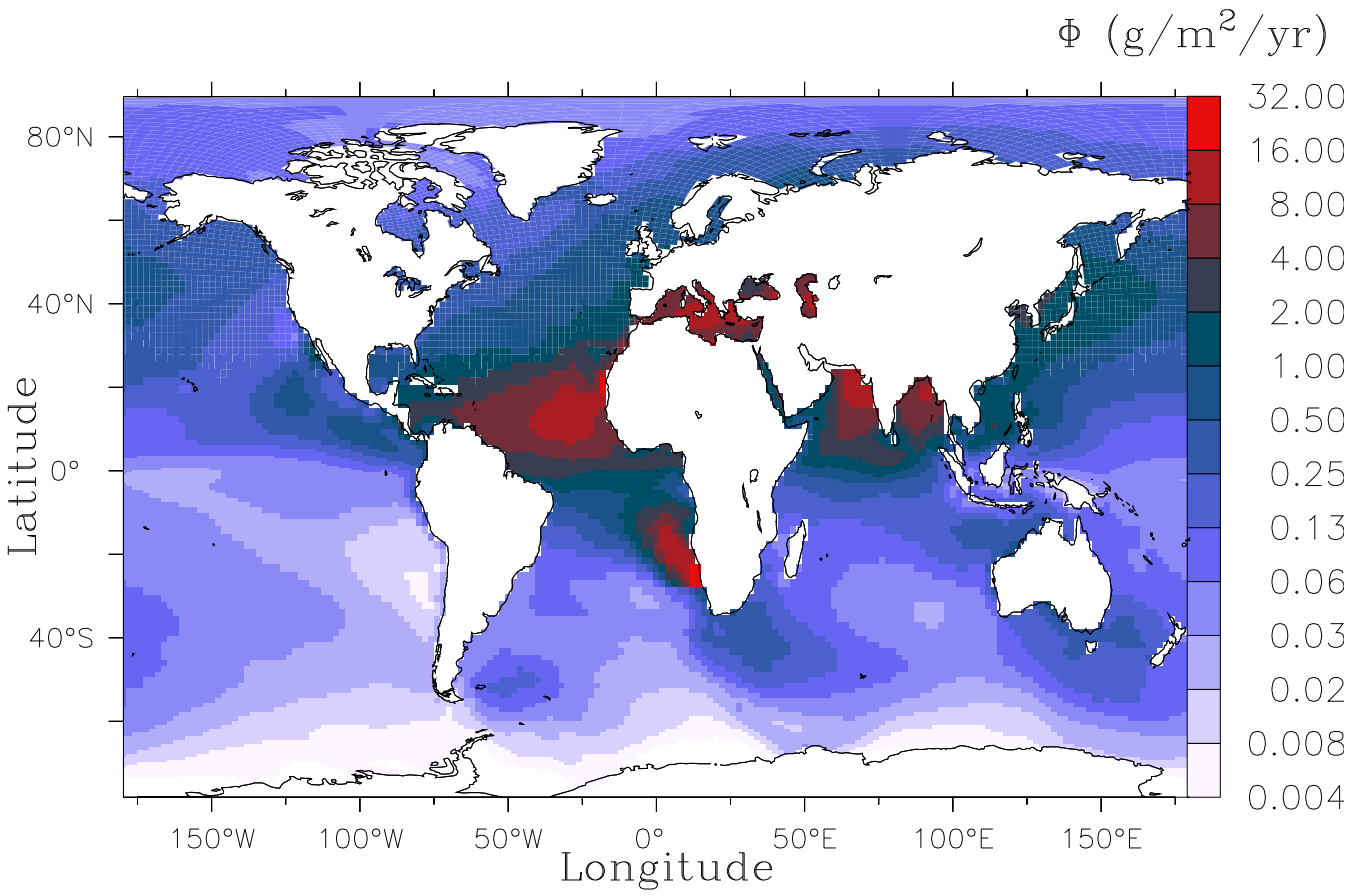

Figure 2. Dust deposition on a logarithmic scale ($\mathrm{g\,m^{-2}\,a^{-1}}$). It is the integrated flux over the 12-months climatology based on Hauglustaine et al. (2004).

ocean, and do not change much over time (Ku et al., 1977). The residence time of $^{234}\mathrm{U}$ is 3.2–5.6 $\times\, 10^5$ a, which is much longer than the full mixing time of the world ocean of about 10^3 a (Dunk et al., 2002). The $^{234}\mathrm{U}$ concentration can vary about 10 %, depending mostly on the salinity (Owens et al., 2011), but that is smaller than uncertainties arising from other assumptions in our model. Therefore, we assume that the production rates of $^{230}\mathrm{Th}$ and $^{231}\mathrm{Pa}$ are constant, both in space and time.

The $^{230}\mathrm{Th}$ and $^{231}\mathrm{Pa}$ radionuclides are reversibly scavenged by biogenic and lithogenic particles (Fig. 3). We will assume, as in previous studies (e.g. Siddall et al., 2005; Dutay et al., 2009), that the adsorption and desorption reaction rates are much faster than radionuclide production, decay, advection, mixing, change in particle distribution and settling of the adsorbed phases. Because of that, we equilibrate between the dissolved and adsorbed phases instantly at each time step. This means,

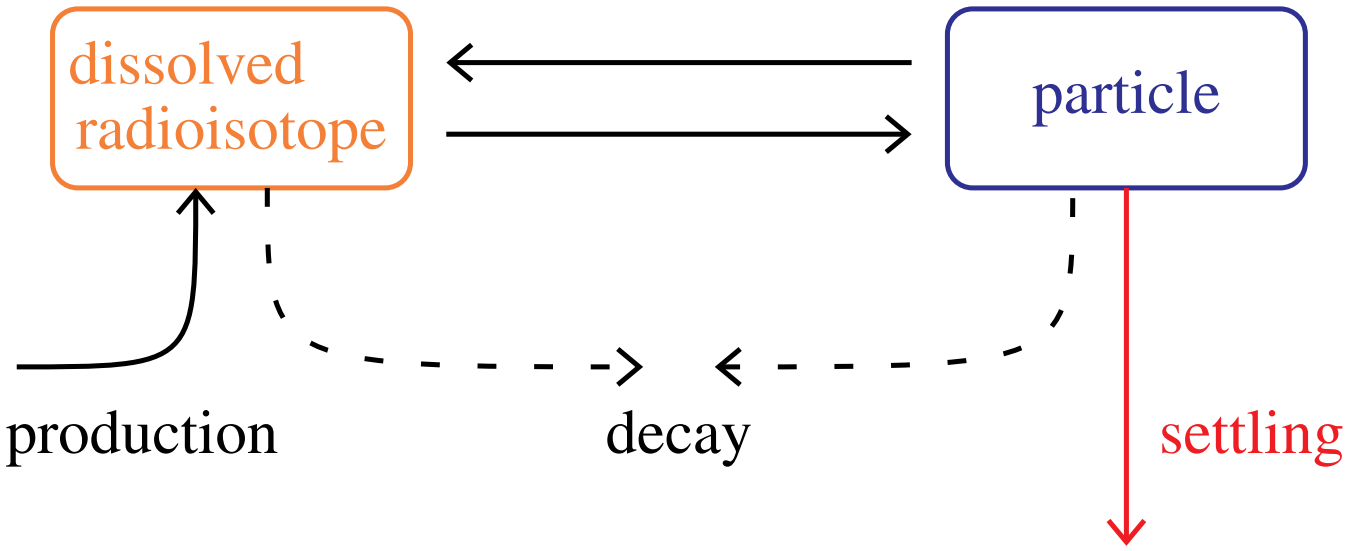

Figure 3. The conceptual reversible scavenging model for the radionuclides. The radioisotopes, $^{230}\mathrm{Th}$ and $^{231}\mathrm{Pa}$, are depicted in orange when in the dissolved phase. Just like with the other PISCES tracers, the dissolved and particulate radionuclides are transported by circulation and eddy diffusion.

only considering ad- and desorption processes at this point, that we must solve this set of equations for every nuclide i:

$$0 = \frac{\partial}{\partial t}(A_{i,D} + A_{i,S} + A_{i,B}), \tag{7a}$$

$$A_{i,S} = A_{i,D} \sum_{j \in S} K_{ij} P^j, \tag{7b}$$

$$A_{i,B} = A_{i,D} \sum_{j \in B} K_{ij} P^j, \tag{7c}$$

where A_i stands for the activity of nuclide $i \in \{^{230}\mathrm{Th}, ^{231}\mathrm{Pa}\}$,[1] and where P^j stands for the concentration of particle $j \in \{\mathrm{sPOC}, \mathrm{bPOC}, \mathrm{CaCO_3}, \mathrm{bSiO_2}, \mathrm{sLitho}, \mathrm{bLitho}\}$ (in gram per gram of seawater, so strictly this is a *mass fraction*). D is the set of non-sinking phases (here only dissolved), S of small particles that sink with $2\ \mathrm{m\,d^{-1}}$ and B of big particles that sink with $50\ \mathrm{m\,d^{-1}}$ (in the same way as Eq. (6) for lithogenic particles). For any particle size class $J \in \{S, B\}$ and any radionuclide i, we define $A_{i,J} = \sum_{j \in J} A_{ij}$. Finally, K_{ij} is the equilibrium partition coefficient of nuclide i for particle j.

Since we cannot solve this analytically, this will be done numerically by first assigning a new value to the dissolved nuclide activity:[2]

$$A_{i,D} := \frac{A_{i,D} + A_{i,S} + A_{i,B}}{1 + \sum_j K_{ij} P^j}. \tag{8}$$

[1] Concentration of radionuclides (amount per unit of volume) is proportional to its (radio)activity (disintegrations per unit of time). These terms are used interchangeably throughout this paper. Moreover, they are considered identical: the activity or concentration $[^{230}\mathrm{Th}]_D \equiv A_{^{230}\mathrm{Th}}$ is expressed in $\mathrm{mBq\,m^{-3}}$, and thus we report activity ratios of $^{231}\mathrm{Pa}/^{230}\mathrm{Th}$.

[2] When summation bounds are not specified, the union of all phases, $D \cup S \cup B$, is assumed.

Then, we calculate the activity of i that is adsorbed onto small and big particles by applying Eqs (7b) and (7c). With this approach, the small and big adsorbed concentrations equilibrate instantly. Assuming that the change in adsorption strength is much smaller than the relative change in tracer activity, $\forall_{i,J:}\partial_t \sum_{j\in J} K_{ij}P^j \ll \partial_t A_{i,D}/A_{i,D}$, the total activity of every i is conserved, i.e. Eq. (7a) holds.

Proof. Let the total adsorption strength for any isotope i be $Q_i = \sum_j K_{ij}P^j$ and the total amount of the same isotope $T_i = A_{i,D} + A_{i,S} + A_{i,B}$, and let primes denote the updated concentrations. Assume that the adsorption strength for every isotope i is constant ($Q'_i \equiv Q_i$).

$$\begin{aligned} T'_i &= \frac{T_i}{1+Q'_i} + A'_{i,D}Q'_i \\ &= \frac{T_i}{1+Q_i} + \frac{T_i}{1+Q_i}Q_i \\ &= \frac{T_i}{1+Q_i}(1+Q_i) = T_i \end{aligned}$$

$$\Rightarrow \partial_t T'_i = \partial_t T_i = 0\,. \qquad \square$$

The $^{230}\mathrm{Th}$ and $^{231}\mathrm{Pa}$ that are adsorbed onto the particles follow the same law as the small and big (lithogenic) particles (Eq. 6). Of course, by definition, the adsorbed radioisotope and the particle settle with the same speed, and thus we have implemented it.

The decay terms of $^{230}\mathrm{Th}$ and $^{231}\mathrm{Pa}$ are much smaller than the other sources and sinks, but they are included in the model:

$$\frac{\mathrm{d}A_{i,D}}{\mathrm{d}t} = \beta_i - \lambda_i A_{i,D} + (\mathcal{A}\nabla_h^2 + \mathcal{B}\frac{\partial^2}{\partial z^2})A_{i,D}\,, \tag{9a}$$

$$\frac{\mathrm{d}A_{i,S}}{\mathrm{d}t} = -\lambda_i A_{i,S} - w_s\frac{\partial A_{i,S}}{\partial z} + (\mathcal{A}\nabla_h^2 + \mathcal{B}\frac{\partial^2}{\partial z^2})A_{i,S}\,, \tag{9b}$$

$$\frac{\mathrm{d}A_{i,B}}{\mathrm{d}t} = -\lambda_i A_{i,B} - w_b\frac{\partial A_{i,B}}{\partial z} + (\mathcal{A}\nabla_h^2 + \mathcal{B}\frac{\partial^2}{\partial z^2})A_{i,B}\,, \tag{9c}$$

where β_i and λ_i are respectively the production rate and radioactive decay of isotope i.

3 Simulations

For the numerical simulations, we forced the just described model, an adjusted version of PISCES with lithogenic particles and radiotracers, with the off-line circulation fields. The model was spun up for 500 yr, after which it was in an approximate steady state (decadal drift of $-0.002\,\%$ for total $^{230}\mathrm{Th}$ and $+0.058\,\%$ for total $^{231}\mathrm{Pa}$). Protactinium-231 has a larger drift than thorium-230, because $^{230}\mathrm{Th}$ is everywhere in the ocean more quickly removed because of its high particle reactivity. The lithogenic particles are in a steady state, and the PISCES variables are in an approximate steady state (e.g. phosphate shows a drift of $-0.005\,\%$ per decade.

The partition coefficients K_{ij}, with $i \in \{\mathrm{Th}, \mathrm{Pa}\}$, depend on the type of particle j and are given in Table 2. These coefficients have large uncertainties still, but their values can be constrained by reported values from different experimental studies (e.g.

Particle	K_{Pa} $(\mathrm{Mg\,g^{-1}})$	K_{Th} $(\mathrm{Mg\,g^{-1}})$	Settling speed
small POC	2.0	5.0	$2\ \mathrm{m\,d^{-1}}$
big POC	0.4	1.0	$50\ \mathrm{m\,d^{-1}}$
biogenic silica	0.5 (0.4)	0.5 (1.0)	$50\ \mathrm{m\,d^{-1}}$
$\mathrm{CaCO_3}$	0.12	5.0	$50\ \mathrm{m\,d^{-1}}$
small lithogen.	10.0	50.0	$2\ \mathrm{m\,d^{-1}}$
big lithogen.	1.0	5.0	$50\ \mathrm{m\,d^{-1}}$

Table 2. Partition coefficients for the different modelled particles in 10^6 gram of seawater per gram of particles. Between braces is the value for the sensitivity simulation discussed in Section 6.1.

Chase et al., 2002; Geibert and Usbeck, 2004; Hayes et al., 2015b). Therefore, we had quite some freedom in prescribing values. The adsorption onto calcium carbonate is a factor two decreased from Chase et al. (2002). This brings the K value of Pa closer to that in Hayes et al. (2015b) based on field measurements, namely $0.9 \pm 0.4\ \mathrm{Mg\,g^{-1}}$ (10^6 gram of seawater per gram of particles), but since we maintained the ratio of K values, the partition coefficient of Th is much smaller than found by Hayes et al. (2015b). It is consistent with the laboratory results of Geibert and Usbeck (2004), but they cleaned the opal aggresively, bought carbonate that should be organic-free and clay (smectite) was purchased as a commercial standard and not cleaned (Geibert and Usbeck, 2004, as well as pers. comm. January 2018). In the real ocean, solid minerals are not clean but have organic matter around them, giving rise to increase scavenging (Chuang et al., 2014, for diatoms). Therefore, our K's for at least biogenic silica and calcium carbonate may be lower than what is typically considered realistic. The actual reason for the relatively low K values is that we only have fast sinking biogenic silica and calcium carbonate particles in the model that represent also smaller particles that sink slower. Thus using higher K values would result in too much export of Pa and Th. For small lithogenic particles, K is set about a factor five larger than literature (Geibert and Usbeck, 2004; Hayes et al., 2015b), whereas big lithogenic particles have a smaller value than reported in the literature. The supplementary document contains a more exhaustive table of information, including an estimated literature range (Table S3). The consequences of chosen values of the partition coefficients is discussed further in Section 6.

4 Observations

In this study, we will focus on the GEOTRACES GA03 transect in the North Atlantic Ocean. Recently, a large number of measurements on both radionuclides and their carrier particles have been collected on this transect. This unique combination makes it especially useful to evaluate a radionuclide scavenging model. We will also compare our global ocean model with several observational datasets throughout the ocean (Table 3). Observations obtained from the GEOTRACES programme are denoted with the respective GEOTRACES transect number (Mawji et al., 2015).

Transect	Year	Expedition	Ocean basin	Citation
Carrier particles POC, $CaCO_3$, $bSiO_2$ and lithogenic				
–	1973–74	GEOSECS st.235,239,306	Central Pacific	Brun-Cottan et al. (1991)
–	1985–91	Alcyone-5, Eve-1, Hydros-6	North Pacific	Druffel et al. (1992)
–	1982–97	WCR, Line P, SOFeX, K2, JGOFS	Pacific and Atlantic	Lam et al. (2011)
GA03	2011	US GT10 and GT11	North Atlantic	Lam et al. (2015)
Radionuclides ^{230}Th and ^{231}Pa				
–	1979	R/V *Knorr* cruise 73/leg 16	Central-east Pacific	Bacon and Anderson (1982)
–	1994	R/V *Moana Wave*, HOT-57	Central Pacific	Roy-Barman et al. (1996)
–	1976–98	(multiple)	global	Henderson et al. (1999)
–	1983–02	(multiple)	global	Marchal et al. (2007)
GIPY5_w	2008	ANT XXIV/3	Southern Ocean / Drake	Venchiarutti et al. (2011)
GIPY5_e	2008	ANT XXIV/3	Southern Ocean / Zero merid.	Venchiarutti et al. (2011)
–	2009	SO202-INOPEX, ALOHA, SAFe	North Pacific	Hayes et al. (2013)
GA02	2011	JC 057	Southwest Atlantic Ocean	Deng et al. (2014)
GA03	2010	US GT10 and GT11	North Atlantic	Hayes et al. (2015b)
Sediment top core $^{231}Pa/^{230}Th$				
–	1966–97	(multiple)	global	http://climotope.earth.ox.ac.uk/data_compilations
–	2009	R/V *M. Dufresne*, MD173/RETRO3	global	Burckel et al. (2015, 2016)

Table 3. Observations used for comparison with the model simulations.

For the carrier particles most of our data come from Lam et al. (2015), which is a recent GEOTRACES dataset at the GA03 transect in the North Atlantic Ocean. An older compilation of particles is taken from Lam et al. (2011). We use some older data as well (Table 3). Particle concentrations were determined by filtering seawater in situ.

Concentrations of both dissolved and particulate phases of ^{230}Th and ^{231}Pa were taken from Hayes et al. (2015a) (GA03) and Hayes et al. (2014) (Pacific Ocean). Other data are listed in Table 3.

To evaluate the sediment $^{231}Pa/^{230}Th$ flux of the model, we will compare with compilations of the Holocene (i.e. top core particulate concentrations) (Table 3).

5 Results

5.1 Circulation

As mentioned before, our model is part of a global general circulation model, but instead of solving the Navier-Stokes equations, our tracers are advected by the circulation fields of a previous simulation of the dynamical ocean model. Since the overturning circulation is of importance for the redistribution of the tracers, we here present basic results.

Figure S1 of the supplementary document presents the Overturning Stream Function (OSF) of the Atlantic Ocean. The OSF is defined as the zonally (through the basin) and vertically (from the surface downwards) integrated meridional current speed. We use this as a measure for the Atlantic Meridional Overturning Circulation (AMOC). The upper overturning cell transports 14 Sv (1 Sv $= 10^6$ m^3 s^{-1}) on average. Observations suggest higher values of about 19 ± 5 Sv (Cunningham et al., 2007; Rayner et al., 2011; Sinha et al., 2018). The lower cell has an overturning strength of about 6 Sv, which is stronger than the about 2 Sv from estimates (e.g. Talley et al., 2003). This overestimation is mostly due to the fact that the AMOC is shallow. The AMOC reaches about 2500 m depth, whereas observational studies show the deep water sinks down to about 4000 m. At around 30° N the AMOC has weakened notably, which is consistent with some studies (e.g. Johnson, 2008), but the Antarctic Bottom Water (AABW) does not go as far north as other studies suggest (e.g. 45° N in Van Aken, 2011).

The Antarctic Circumpolar Current is also an important feature for large-scale ocean circulation. The through-flow at Drake Passage is a good measure for that. In our model the flux through Drake Passage is 200 Sv, which slightly overestimates recently reported values (e.g. 173 ± 11 Sv in Donohue et al., 2016).

5.2 Particles

Figure 4 shows the surface concentrations of total POC, big calcium carbonate, big biogenic silica and total lithogenic particles. Observations are plotted as coloured discs on top of the modelled concentrations. The modelled biogenic particles include living matter. For the model, we assume POC includes all phytoplankton and microzooplankton (not mesozooplankton since it may swim away), calcium carbonate contains the assumed fraction of $CaCO_3$ in the phytoplankton, and biogenic silica includes living diatoms. The modelled concentrations and patterns of total POC compare well with the observations (Fig. 4a). For instance, coastal and equatorial Pacific POC concentrations are both in the model and the observations elevated compared to other regions, albeit that the spatial extent of the oligotrophic regions appears to be too small in the model. We compare our modelled $CaCO_3$ (big, fast-sinking, calcium carbonate particles), with the big calcium carbonate particles from observations. As the model tries to represent $CaCO_3$ with only one size class, neither comparing with only big particles nor comparing with total $CaCO_3$ is completely fair. Incidentally, we have data of big $CaCO_3$ for both the Atlantic and Pacific Ocean, whereas we only have small particle data for the Atlantic Ocean. Even though the meridional patterns of big $CaCO_3$ particles are reproduced, its concentrations are generally overestimated, especially in the Gulf of Alaska (Fig. 4b). Contrarily, *total* observed $[CaCO_3]$, which includes smaller particles, of which measurements are available only at GA03, is higher than the prediction of our modelled (only big) $CaCO_3$ particle concentration. The model produces a reasonable spatial distribution of

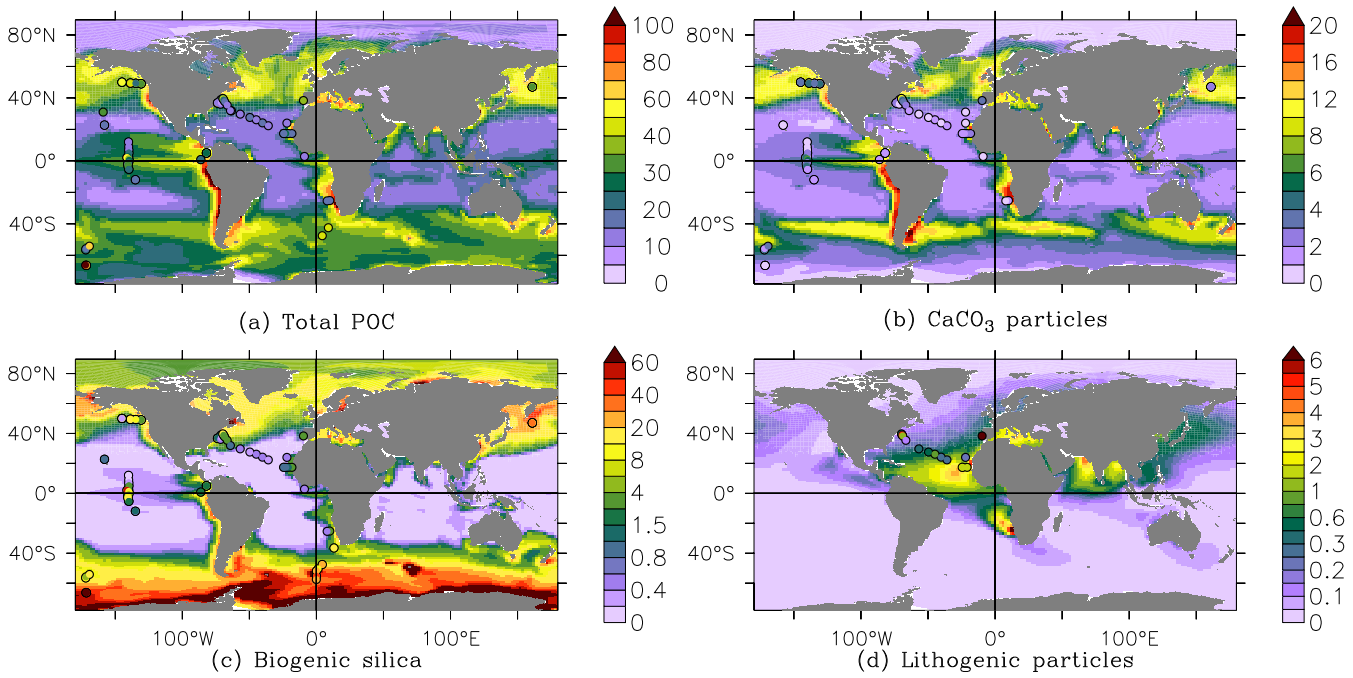

Figure 4. Particle concentrations from the PISCES model at the surface ocean. Observations are represented as coloured discs (Brun-Cottan et al., 1991; Druffel et al., 1992; Lam et al., 2011, 2015). The unit of every modelled and measured particle concentrations is $\mathrm{mg\,m^{-3}}$.

biogenic silica: there are more elevated values in the high latitudes, but concentrations are underestimated at the surface at low latitudes (Fig. 4c).

The recent large dataset obtained from the full-ocean depth GEOTRACES GA03 transect (Lam et al., 2015) provides an opportunity to analyse the performance of PISCES in more detail. PISCES generally produces the right order of magnitude for all four biogenic particles (small and big POC, calcium carbonate and biogenic silica), but there still remain some shortcomings in their distributions (Fig. 5a–d).

- The total POC concentration in Fig. 5a is up to a factor of 4 underestimated in the deep oligotrophic ocean. In the upper $200\ \mathrm{m}$ of the ocean the model overestimates the observations, though at some points at the surface the POC concentration is underestimated (also Fig. 4a). In both the observations and the model the fraction of big POC varies from zero to 0.6 (Fig. 5b), but the spatial distributions are very different. More detailed results and discussion on the simulation of POC are to be found in Aumont et al. (2017).

- The model underestimates the $\mathrm{CaCO_3}$ concentrations from 70° W to 25° W by a factor of 2 to 10, but east of that up to Africa the prediction lies close to or overestimates the observations. In the Canary Basin and up to Portugal (meridional transect at the right), the model reproduces the right order of magnitude, but it does not reproduce the correct profiles everywhere (Fig. 5c).

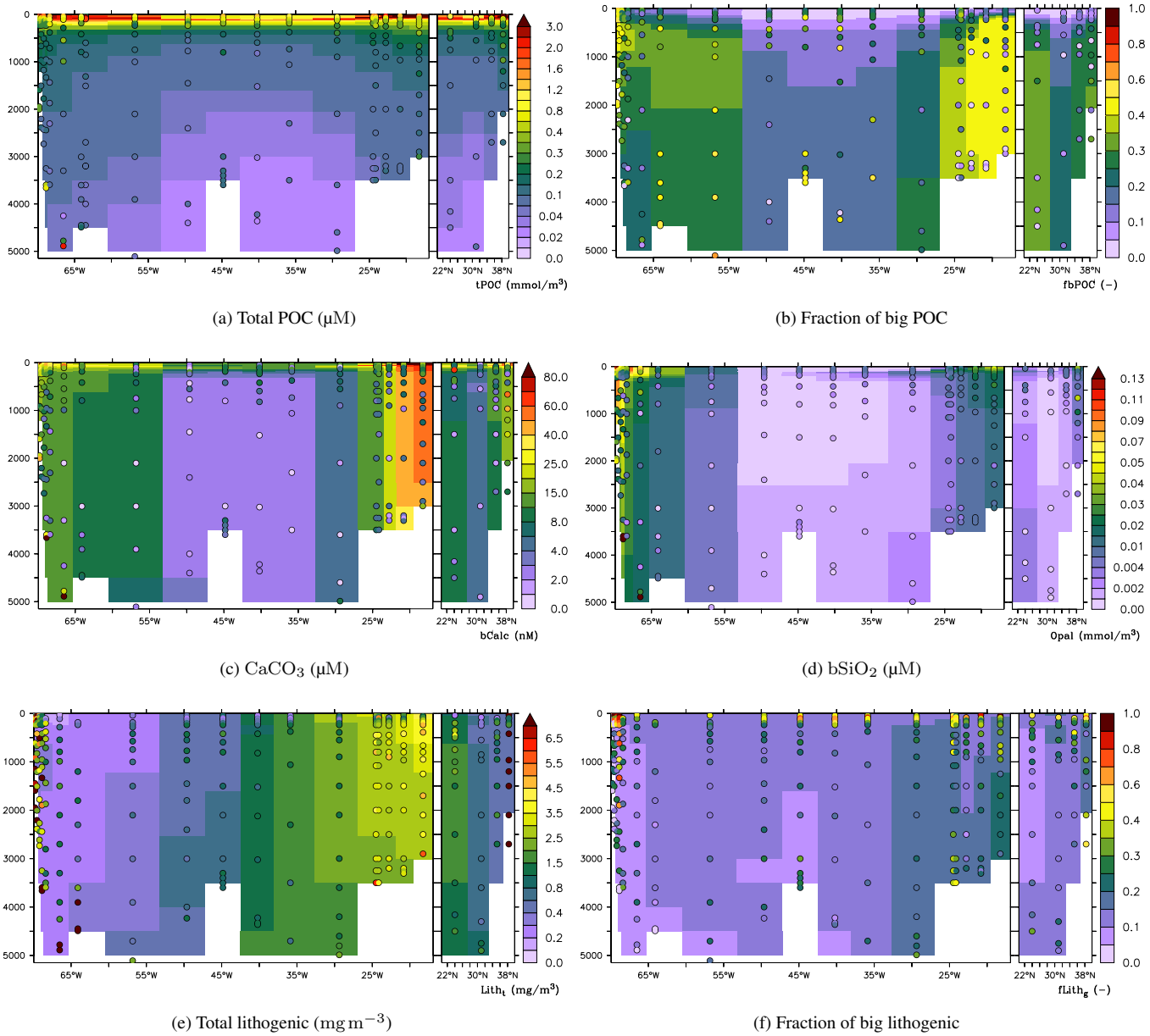

(a) Total POC (µM)

(b) Fraction of big POC

(c) $CaCO_3$ (µM)

(d) $bSiO_2$ (µM)

(e) Total lithogenic ($mg\,m^{-3}$)

(f) Fraction of big lithogenic

Figure 5. Particle fields at the GA03 North Atlantic GEOTRACES transect; observations (Lam et al., 2015) as coloured discs.

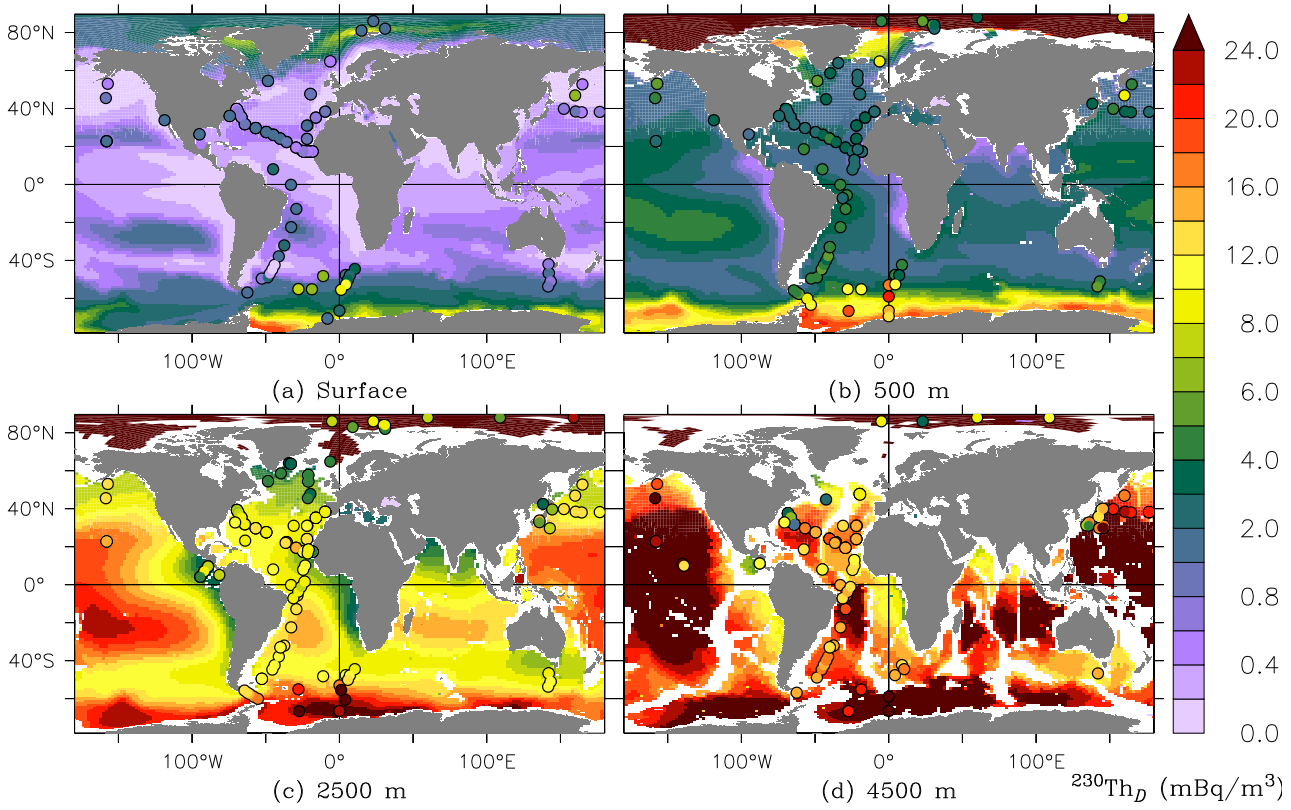

Figure 6. The dissolved thorium-230 activity at four depth levels ($\mathrm{mBq\,m^{-3}}$), observations as discs at the same colour scale.

– Biogenic silica concentrations are generally reproduced but the model overestimates the higher concentrations observed along the western margin (Fig. 5d).

Finally, the modelled total lithogenic particle concentration at the surface shows, as expected, a close resemblance with dust deposition patterns (Fig. 2), and mostly compares well with observations (Fig. 4d). Only near the coasts of the USA and of Portugal the model strongly underestimates lithogenic particle concentrations. Concerning the deep ocean, our model captures quite nicely the general distribution at the GA03 transect (Figs. 5e and 5f). However, the concentrations near the western boundary are strongly underestimated, especially those of big lithogenic particles. Our model reproduces the observed fraction of big lithogenic particles of ∼0.1 to about ∼0.3 in most of the deep ocean, but it underestimates the much larger fraction of big particles observed in the upper 200 m of the ocean (0.1–0.2 in the model versus 0.3–0.9 in the observations).

5.3 Thorium-230 and protactinium-231

$[^{230}\mathrm{Th}]_D$ stands for the concentration of $^{230}\mathrm{Th}$ that is in the dissolved phases. Similarly, $[^{230}\mathrm{Th}]_S$ is the concentration of $^{230}\mathrm{Th}$ that is adsorbed onto the small particles S, $[^{230}\mathrm{Th}]_B$ the concentration adsorbed onto the big particles B; and similarly for $^{231}\mathrm{Pa}$. The modelled dissolved distributions of $^{230}\mathrm{Th}$ and $^{231}\mathrm{Pa}$ are underestimated at the surface (Figs 6 and 7). Below the

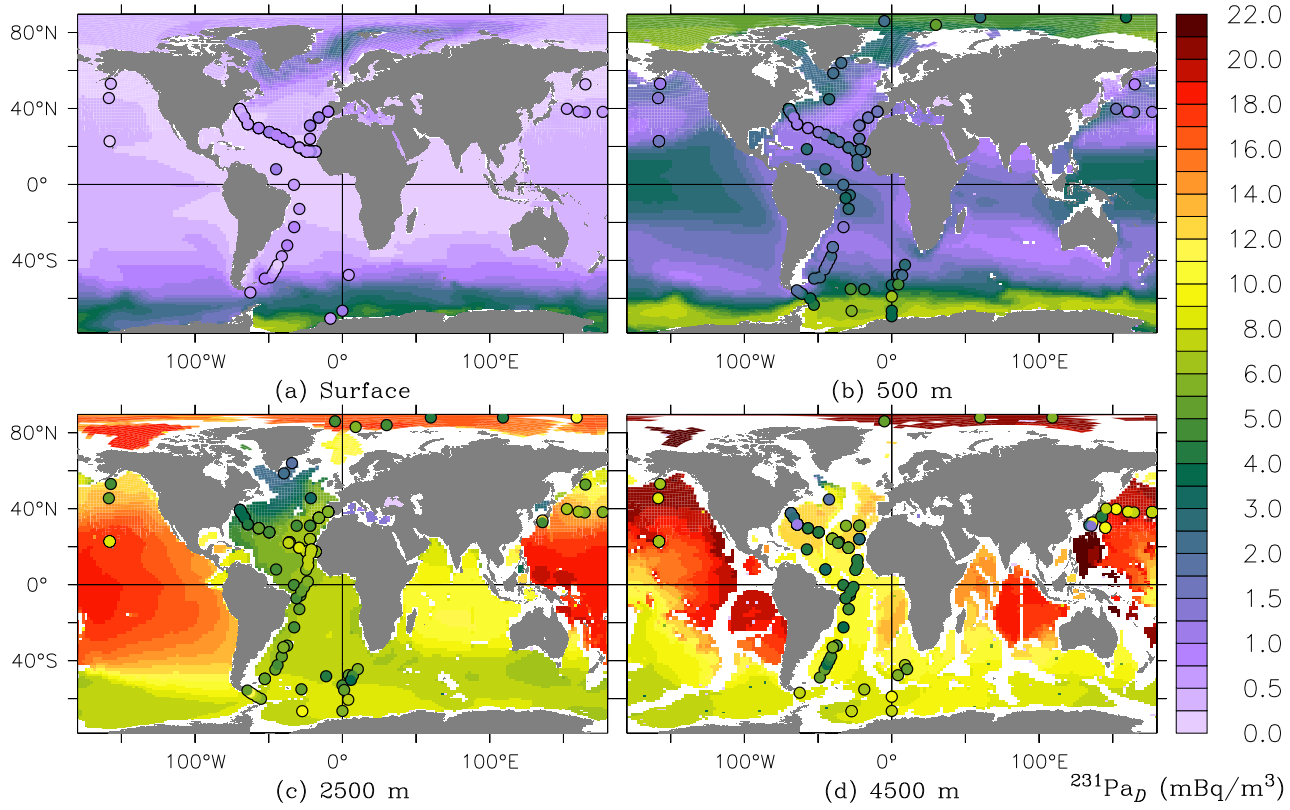

Figure 7. The dissolved protactinium-231 activity at four depth levels ($\mathrm{mBq\,m^{-3}}$), observations as coloured discs.

surface, $[^{230}\mathrm{Th}]_D$ is much better captured by the model (also Fig. 8a for the GA03 transect). However, observations show lower values near the bottom in the western part of the GA03 section and at 45° W, associated with more intense scavenging related to respectively nepheloid layers and manganese oxides from hydrothermal vents, which are not produced in the simulation (Figs 8a and 8b).

In the intermediate and deep waters of all the oceans, modelled $[^{231}\mathrm{Pa}]_D$ is generally of the correct order of magnitude but is strongly overestimated below 2500 m depth (Fig. 8b), especially in the Pacific Ocean (Fig. 7c,d).

The concentrations of the adsorbed phases of $^{230}\mathrm{Th}$ at GA03 are presented in Figs 8c and 8e. In the deep ocean, modelled $[^{230}\mathrm{Th}]_S$ and $[^{230}\mathrm{Th}]_B$ have lower values than $[^{230}\mathrm{Th}]_D$, which is consistent with observations. Furthermore, compared with Dutay et al. (2009), we have notably improved $[^{230}\mathrm{Th}]_S$ and $[^{230}\mathrm{Th}]_B$. Other global modelling studies have not reported adsorbed concentrations of $[^{230}\mathrm{Th}]_D$ and $[^{231}\mathrm{Pa}]_D$. However, the model still underestimates the observed $[^{230}\mathrm{Th}]_S$ and $[^{230}\mathrm{Th}]_B$.

Contrarily, small $^{231}\mathrm{Pa}$ particles are overestimated in our model below 1500 m at the GA03 transect (Fig. 8d). Big $^{231}\mathrm{Pa}$ particles are simulated more realistically (Fig. 8f).

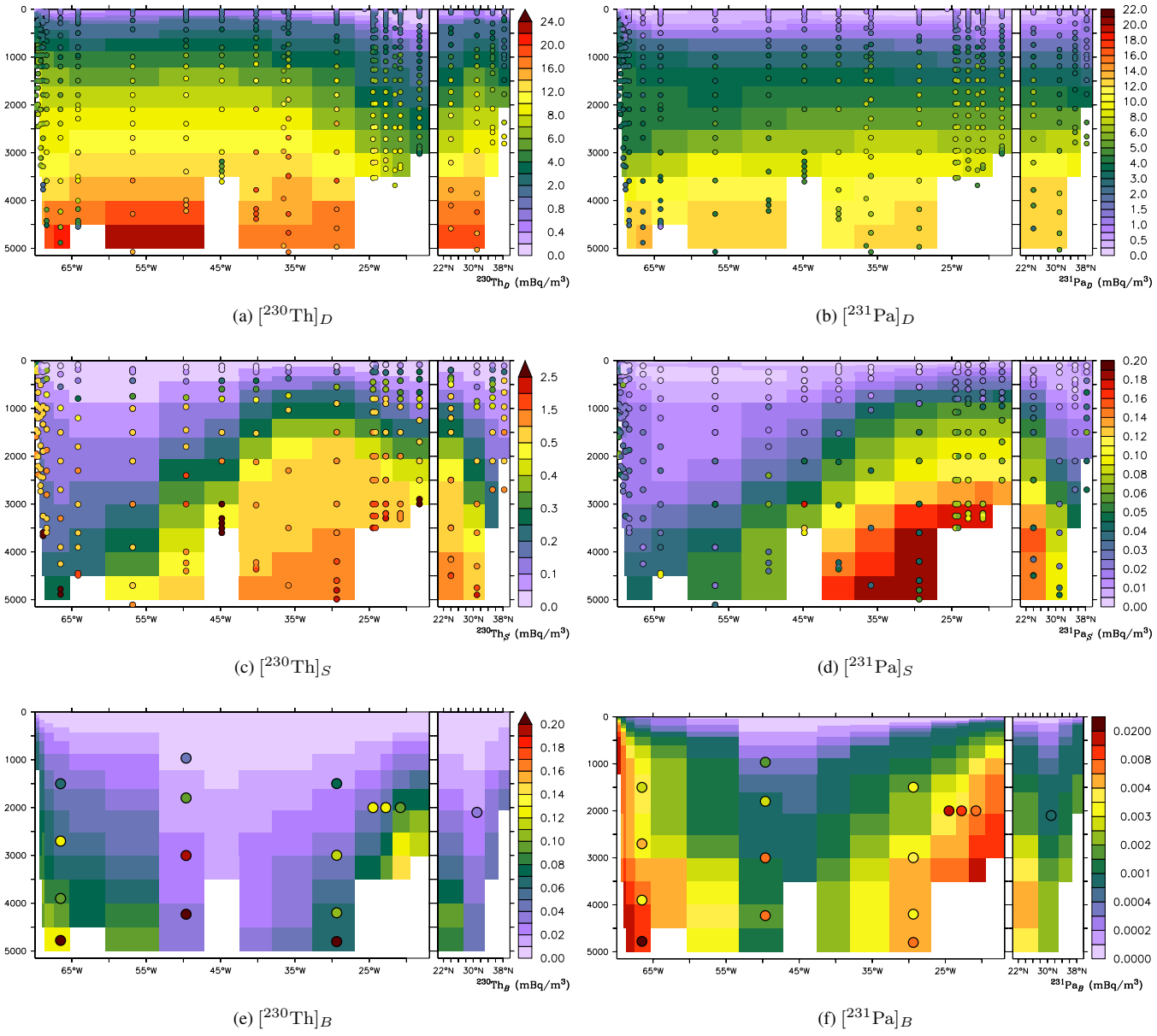

(a) $[^{230}\mathrm{Th}]_D$

(b) $[^{231}\mathrm{Pa}]_D$

(c) $[^{230}\mathrm{Th}]_S$

(d) $[^{231}\mathrm{Pa}]_S$

(e) $[^{230}\mathrm{Th}]_B$

(f) $[^{231}\mathrm{Pa}]_B$

Figure 8. Radionuclide concentrations at the GA03 North Atlantic GEOTRACES transect. (a) and (b) display dissolved concentrations, (c) and (d) show the amounts on small particles, and (e) and (f) those on big particles. Everything is in ($\mathrm{mBq\,m^{-3}}$). Observations (Hayes et al., 2015a) are shown as coloured discs.

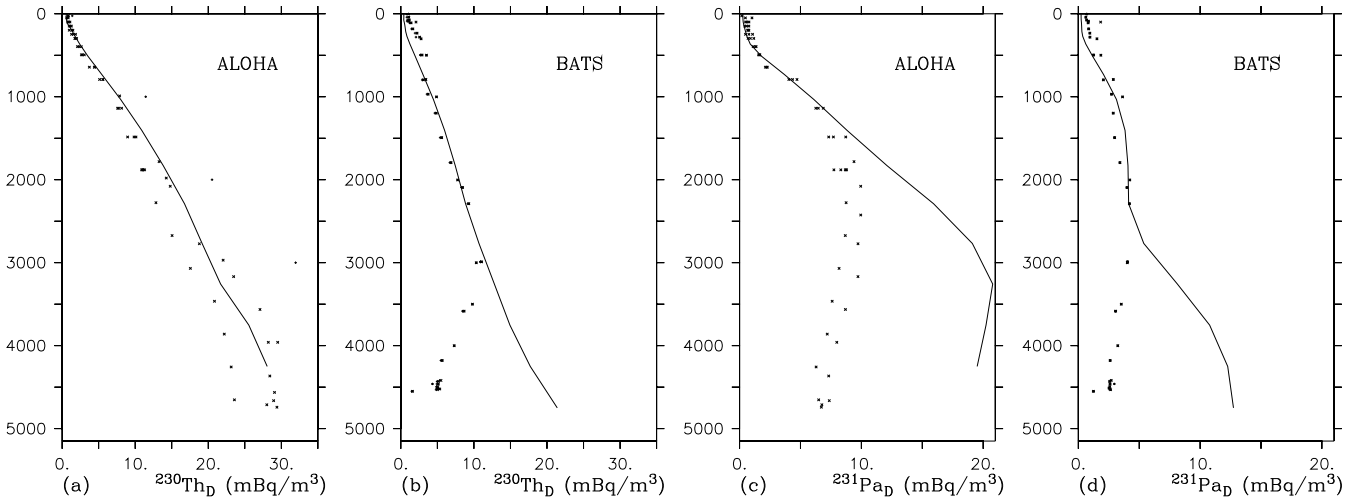

Figure 9. Radionuclide concentrations in $\mathrm{mBq\,m^{-3}}$ at stations in the North Pacific (around ALOHA station, 158° W, 23° N) and North Atlantic Oceans (around the BATS station, 64° W, 29° N). The left two panels (a,b) display $[^{230}\mathrm{Th}]_D$, and the right two (c,d) $[^{231}\mathrm{Pa}]_D$. The line is the model, and the speckles are the observations.

%		POC	$\mathrm{bSiO_2}$	$\mathrm{CaCO_3}$	Litho.
	global stock	35.5	10.5	3.1	50.8
$^{231}\mathrm{Pa}$	global particle flx	16.5	53.5	15.8	14.2
	North Atlantic flx	16.5	25.7	15.6	42.1
	Southern Ocean flx	5.6	93.7	0.6	0.1
	global stock	21.3	3.2	24.3	51.2
$^{230}\mathrm{Th}$	global particle flx	5.9	9.9	75.8	8.7
	North Atlantic flx	4.4	2.8	69.9	22.9
	Southern Ocean flx	9.7	71.1	18.9	0.3

Table 4. Relative global budget of $^{231}\mathrm{Pa}$ and $^{230}\mathrm{Th}$ in the different particulate phases ("global stock") in percentages. Globally averaged fluxes in the different phases ("global particle flx"), and the same but for the North Atlantic Ocean (44–24° W, 25–56° N) and the Weddell Sea (44–24° W, 76–63° S), all in percentages associated with each particle type.

To show clearly the change of $[^{230}\mathrm{Th}]_D$ and $[^{231}\mathrm{Pa}]_D$ with respect to depth, profiles are plotted in Fig. 9. $[^{230}\mathrm{Th}]_D$ is linearly increasing downwards, which matches with the observations, but below 3000 m near Bermuda, $[^{230}\mathrm{Th}]_D$ increases where it should decrease according to the observations. The shape of $[^{231}\mathrm{Pa}]_D$ matches that of the observations for the upper 2 km, below which our model overestimates the observations up to a factor four at the bottom of the ocean.

Globally in the model, only 0.3 % of the $^{231}\mathrm{Pa}$ sits in the particulate pool, and for $^{230}\mathrm{Th}$ this is 1.3 %. The rest is in the dissolved phase. Observational data show that more than 10 % of $^{230}\mathrm{Th}$ sits in the particulate pool, typically adsorbed onto small calcium carbonate particles. The underestimation by our model can be explained by the fact that we only have big, fast-sinking $\mathrm{CaCO_3}$ particles in the model. Since the big particles are removed quickly, these cannot act as a realistic $\mathrm{CaCO_3}$-associated $^{230}\mathrm{Th}$ pool without depleting $^{230}\mathrm{Th}$, and thus we underestimate the particulate radionuclide concentrations.

Table 4 gives two types of information on the adsorbed phases. One is the amount fraction of radionuclide adsorbed onto each particle ("global stock"). The other is the fraction of the flux carried by each type of particle (the other rows) for the global ocean and two regions of the ocean. No distinction is made between big and small particles (they are summed). The stock and the flux are not necessarily the same, because the big particles have a different settling velocity from the small particles. For example, only for POC and lithogenic particles do we have slowly sinking particles on which much of the radionuclides are adsorbed, whereas the big affinity of Pa to $\mathrm{bSiO_2}$ mostly results in a strong export (and similarly for Th on $\mathrm{CaCO_3}$).

Only a small amount of $^{230}\mathrm{Th}$ is adsorbed onto biogenic silica (3 %), though the amount is larger for $^{231}\mathrm{Pa}$ (11 %). However, the global settling flux of $^{231}\mathrm{Pa}$ is primarily (54 %) determined by $\mathrm{bSiO_2}$, particularly due to the high $\mathrm{bSiO_2}$ fluxes in the Southern Ocean. Most of the modelled particulate $^{231}\mathrm{Pa}$ and $^{230}\mathrm{Th}$ is on the lithogenic particles, but lithogenic particles account for only 14 % of the $^{231}\mathrm{Pa}$ flux and 9 % of the $^{230}\mathrm{Th}$ flux. If lithogenic particles from nepheloid layers were included, this fraction would be higher. The flux contribution is also different from what is in the pools when we look at $\mathrm{CaCO_3}$: only 24 % of the $^{230}\mathrm{Th}$ is on calcium carbonate, but $\mathrm{CaCO_3}$ is for 76 % responsible for the $^{230}\mathrm{Th}$ export. These discrepancies between the contribution of each particle type to the flux and to the stock of radionuclides arise from the different speeds for each type of particle.

The relative contributions of the different particulate phases also vary for different regions of the ocean. Opal is for 94 % responsible for $^{231}\mathrm{Pa}$ export in the Southern Ocean.

Compared to Dutay et al. (2009), the improvement of the $^{230}\mathrm{Th}$ profile shape is only to a small extent due to the large improvement in the POC representation (Aumont et al., 2017), because the POC accounts for only 6 % of the vertical transport of $^{230}\mathrm{Th}$ (Table 4). The improvement is mostly due to the addition of lithogenic dust particles and the adjusted $\mathrm{CaCO_3}$ dissolution. Lithogenic particles and $\mathrm{CaCO_3}$ hardly dissolve compared to POC and hence the downward particle flux remains constant, which is in agreement with 1-D models which show linear profiles of $^{230}\mathrm{Th}_D$ (e.g. Roy-Barman, 2009).

5.4 Sedimentation flux ratio of $^{231}\mathrm{Pa}/^{230}\mathrm{Th}$

The sedimentation flux of the total adsorbed $^{231}\mathrm{Pa}/^{230}\mathrm{Th}$ ratio captures the general patterns of the upper sediment core $^{231}\mathrm{Pa}/^{230}\mathrm{Th}$ concentration ratio (Fig. 10). Consistent with observations, the model produces more elevated $^{231}\mathrm{Pa}/^{230}\mathrm{Th}$ ratio values in the Southern Ocean, the northern part of the Indian Ocean, the Pacific Ocean, and along the coastal upwelling regions. However, at some places, like much of the Southern Ocean, our model tends to overestimate the ratio derived from the sediment core observations.

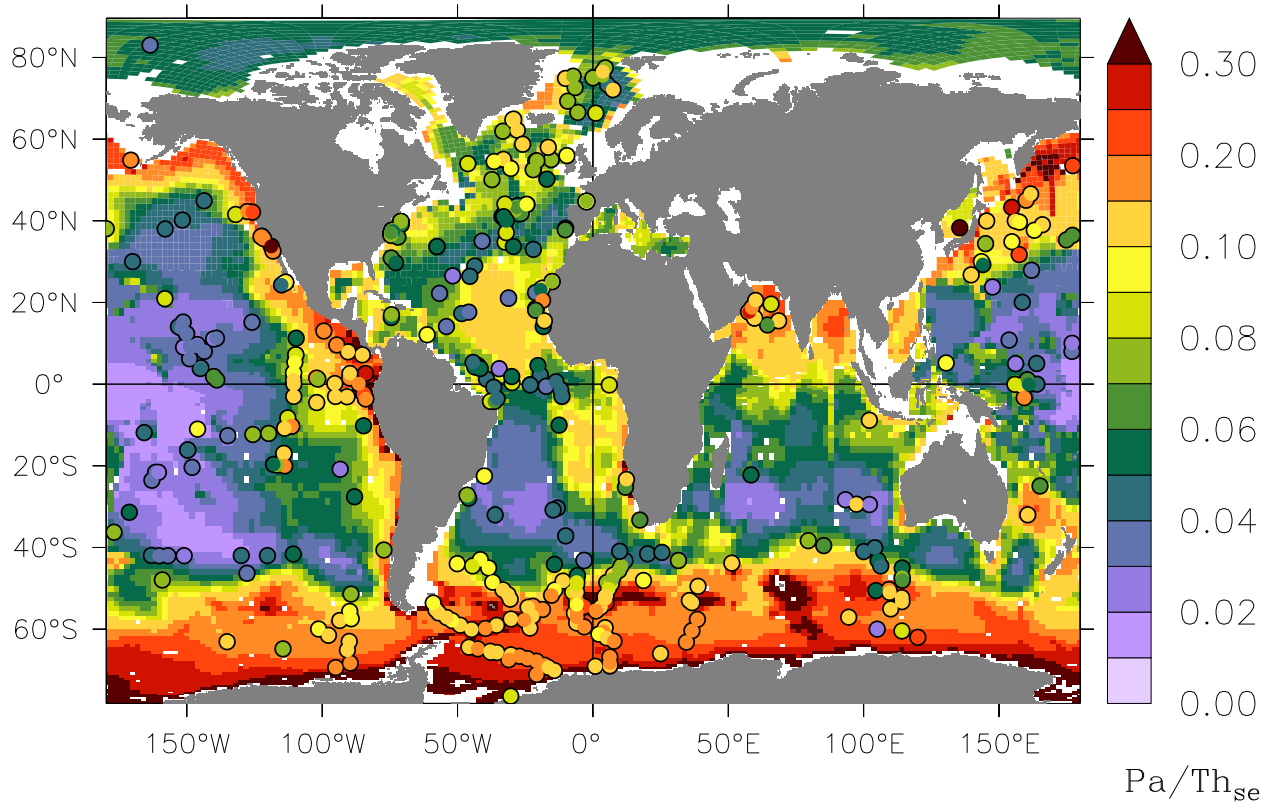

Figure 10. Sedimented ^{231}Pa/^{230}Th ratio. Top core measurements are presented as coloured discs. This is the standard simulation with $K_{\mathrm{Pa,bSiO_2}}/K_{\mathrm{Th,bSiO_2}} = 1$.

6 Discussion

We succeed to generate the global patterns of the dissolved nuclide concentrations. However, we underestimate radioactivities in the surface waters (Figs 7a and 6a). This shortcoming may be due to the instant equilibration between the dissolved and the adsorbed phases (Henderson et al., 1999). After decay of U into ^{231}Pa and ^{230}Th, the tracers instantly adsorb onto the particles in the surface ocean and are exported from the mixed layer. For future model developments, it is of interest to test if a non-instant equilibration model (parameterised with adsorption and desorption coefficients) yield better surface values.

The reversible scavenging model uses partition coefficients K_{ij} for the different isotopes i and particles j. Many studies provide constraints on these coefficients but estimations vary strongly between different studies. Small particles are the most important scavengers and largely control the shape of the vertical profile of the tracers (Dutay et al., 2009). This also shows from sedimentary isotope records (Kretschmer et al., 2011) This is explained by the specific surface of small particles, which is larger than that of big particles. Therefore higher adsorption values are set for small particles compared to the bigger particles of the same type (namely, 5 times higher for POC, and 10 times higher for lithogenic particles). Compared to Dutay et al. (2009),

we succeed to simulate the tracer concentrations using reasonable K values. This is due to improvement in (especially small) particle concentrations, which were generated with the lability parametrisation of POC (Aumont et al., 2017), the change of the $CaCO_3$ dissolution parameterisation, and the addition of lithogenic dust in our ocean model. This shows that at least two particle size classes are needed to simulate dissolved and particulate thorium and protactinium. Our model does not include small particles for all types (there are neither small $CaCO_3$ nor small $bSiO_2$ particles), even though we expect that better results can be reached upon adding those particles akin to small POC and small lithogenic particles.

On the GA02 transect, the correlation coefficient r of the data–model comparison of $[^{230}Th]_D$ is 0.80, which is close to what was reported by Rempfer et al. (2017) in their simulations without bottom-boundary scavenging. On the GA03 section, $r = 0.78$. The correlation between model and observation are presented as scatter plots (supplementary document, Fig. S2).

There are a couple of interesting features to note on the comparisons. Firstly, the hydrothermal plume over the ridge results in ^{230}Th-poor seawater that is not reproduced by the model (red triangle in Fig. S2, GA03). Secondly, in the western boundary currents, very low dissolved ^{230}Th concentrations are observed due to strong nepheloids and/or possibly strong deep ventilation from the north. Neither of these processes are represented in the model. Missing the nepheloids has an especially large impact on the GA02 transect, which has a relatively large number of measured profiles near the western boundary. Finally, between 32 and 20° W, the model tends to underestimate ^{230}Th. The value of the correlation index is not that important, because the goal of this study is not to give a perfect model–data comparison.

The provided dust flux does not distinguish between different dust particle sizes or types. Furthermore, dust deposition is uncertain; therefore we chose a dust flux that was available to the ORCA2 configuration of NEMO, and its biogeochemistry has been tested with that dust flux. However, given the significant impact of dust particles to thorium and protactinium concentrations, it would be useful to look into the effect of different dust deposition fields, and of using different dust particles size classes. A good model of ^{230}Th (and other isotopes of thorium) could even constrain the sporadic and uncertain dust deposition, but all this falls outside the scope of the present study.

Our model adds 80 % of the dust deposition into the fast-sinking lithogenic particle compartment (corresponding to $\varnothing > 51$ µm), and only 20 % goes into the slowly-sinking compartment (corresponding to $\varnothing \leq 51$ µm). This is necessary to reproduce the distributions of lithogenic particles. However, airborne dust particles typically have a diameter of smaller than 20 µm (Knippertz and Stuut, 2014) and thus fall clearly within the small size class of less than 50 µm. Recently, there have been observations of aerosols larger than 20 µm (Van Does et al., 2016), but they do not reach far enough into the atmosphere above the open ocean to explain the high concentration of big lithogenic ocean particles. The explanation for the apparently required high fraction of big lithogenic particles is that smaller aerosols aggregate in the upper layers of the ocean. Moreover, though more hypothetically, there may be strong aggregation with biogenic particles just below the surface, below which the aggregates partly disaggregate again to result in the ∼0.2 big lithogenic fraction in the deep ocean (Fig. 5f).

The underestimation of lithogenic particle concentrations at the western boundary is expected. The reason is that we only have dust deposition as a source of lithogenic particles, whereas nepheloid layers are not included. Nepheloid layers are at least locally an important source of lithogenic (and biogenic) particles (Lam et al., 2015). With the transport of ^{230}Th and ^{231}Pa through the western boundary current, a significant portion may be scavenged. Moreover, the periodic transport through

the North Atlantic Gyre would result in lower $[^{230}\mathrm{Th}]_D$ and $[^{231}\mathrm{Pa}]_D$ throughout a large part of the North Atlantic Ocean, possibly improving the concentrations in the deep ocean. Therefore it will be useful to include nepheloid layers in the future. We have not done this so far, because we do not know how to model nepheloid layers. Except for trivial models, like the one of Rempfer et al. (2017) who forced an additional constant scavenging rate in the bottom box of the ocean model, no large-scale, prognostic nepheloid models have been developed.

We overestimate the radionuclide activity in the deep ocean, which is partly because we underestimate particle concentrations. Especially thorium adsorbs well onto lithogenic particles, which are underestimated in the West Atlantic Ocean (in the subsurface, west of about 43° W, Fig. 5e). Below 2 km depth, also POC is underestimated (Fig. 5a), even though the lability parameterisation improved the distribution by over an order of magnitude compared with previous versions of PISCES (Aumont et al., 2017). Small POC and the small lithogenic particles are the only small particles. Their underestimation in the deep ocean results in an overestimation of the radionuclides in the deep ocean. In our simulation, $[^{230}\mathrm{Th}]_D$ is not that much overestimated (outside the Arctic Ocean). However, $[^{231}\mathrm{Pa}]_D$ is strongly overestimated in the deep Pacific and Atlantic Oceans.

Clearly the model does not remove $^{231}\mathrm{Pa}$ efficiently enough from the deep ocean (Figs 7c,d, 8b and Fig. 12–upper panel). Two likely reasons may be that the waters are not well ventilated in the model (older than in reality), or that there is not enough scavenging. The Atlantic OSF (Fig. **??**) shows that the upper overturning cell is too shallow compared to observational studies, so there is too little ventilation. This means that $^{231}\mathrm{Pa}$ can build up in the deep water due to sluggish ventilation of the physical model (Dutay et al., 2002; Biastoch et al., 2008). Moreover, the AABW has weakened in the deep North Atlantic Ocean near the high-$[^{231}\mathrm{Pa}]_D$ region (Fig. 12–upper panel), which may also contribute to the high dissolved $^{231}\mathrm{Pa}$ concentrations. The volume transport of the lower cell is about 6 Sv near 20° N and still 2 Sv near 40° N, which is in the order of magnitude of what is reported by literature. Moreover, the relationship between sediment $^{231}\mathrm{Pa}/^{230}\mathrm{Th}$ at any given site and the overturning circulation is very complex (Luo et al., 2010). For this reason, it is not obvious whether the weak overturning is large enough to explain the discrepancy between the modelled and the observed $[^{231}\mathrm{Pa}]_D$. In reality, there are many regions in the North Atlantic Ocean where there is sediment resuspension and where there are nepheloid layers (Gardner and Sullivan, 1981; Lam et al., 2015; Gardner et al., 2017). This is consistent with the fact that our model underestimates lithogenic particle concentrations in the West Atlantic Ocean (Fig. 5e). The additional lithogenic particles would scavenge more $^{231}\mathrm{Pa}$, resulting in lower $[^{231}\mathrm{Pa}]_D$. Even though the enforced scavenging occurs near the floor and the western boundary of the ocean, a strong flux of water passes through the latter region, and is transported through the North Atlantic Gyre and through the rest of the Atlantic, diluting high tracer concentrations. The small POC and lithogenic particles are now underestimated in much of the deep ocean. They would contribute to lower radioactivities as well.

Rempfer et al. (2017) confirmed that an additional bottom sink affects $^{231}\mathrm{Pa}$ and $^{230}\mathrm{Th}$ significantly. They used a homogeneous extra scavenger in their model grid's bottom grid cell. Therefore, it would be worth testing if a realistic distribution of nepheloids would result in the right amount of scavenging.

Other particles may include resuspended (nepheloidal) biogenic particles but also manganese and iron hydroxides that are not included in our model, and a smaller class of calcium carbonate and biogenic silica particles in addition to the big-particle classes that are already in the model. Manganese oxides are available especially near hydrothermal vents, but also throughout

the Pacific Ocean in low concentrations but much higher than in the Atlantic Ocean. Indeed, it has been argued that hydrothermal inputs may provide additional removal of $^{231}\mathrm{Pa}$ and $^{230}\mathrm{Th}$ (Lopez et al., 2015; Rutgers van der Loeff et al., 2016; German et al., 2016), and recently this is confirmed based on an analysis of the $\sim 10^{\circ}$ S zonal GP16 transect in the Pacific Ocean (Pavia et al., 2017).

Finally, the particle concentration effect (Honeyman et al., 1988) should be taken into account in future models, especially when those high particle concentration (processes) are to be included in the model.

6.1 Effect of scavenging by $\mathrm{bSiO_2}$ on the $^{231}\mathrm{Pa}/^{230}\mathrm{Th}$ sedimentation flux ratio

Previously, it was suggested that Pa has a stronger affinity for $\mathrm{bSiO_2}$ than Th has, i.e. $F_{\mathrm{Pa/Th,bSiO_2}} > 1$ (Henderson et al., 1999; Chase et al., 2002; Dutay et al., 2009). This "standard view" has weakened over time, so it is often accepted that $F_{\mathrm{Pa/Th,bSiO_2}} \gtrsim 1$ (Venchiarutti et al., 2011; Rutgers van der Loeff et al., 2016; Rempfer et al., 2017). We argue here that it is Th which has the stronger affinity to $\mathrm{bSiO_2}$ ($F_{\mathrm{Pa/Th,bSiO_2}} < 1$), similarly (though not quite) like other particles.

Our standard simulation (with $F_{\mathrm{Pa/Th,bSiO_2}} = 1$) yields a too high sedimentation $^{231}\mathrm{Pa}/^{230}\mathrm{Th}$ ratio compared to top-core sediment observations below diatom-rich areas such as the Southern Ocean. In that region, $\mathrm{bSiO_2}$ largely controls the particle scavenging of the two tracers, especially that of $^{231}\mathrm{Pa}$ (Table 4). In order to estimate how strongly the model depends on the value of the $\mathrm{bSiO_2}$ partition coefficient we performed a sensitivity experiment where we set $K_{\mathrm{Pa,bSiO_2}} = 0.4\,\mathrm{M g\,g^{-1}}$ and $K_{\mathrm{Th,bSiO_2}} = 1.0\,\mathrm{M g\,g^{-1}}$ such that now $F_{\mathrm{Pa/Th,bSiO_2}} = 0.4$ (Table 2).

As a result of this reduction, $^{231}\mathrm{Pa}/^{230}\mathrm{Th}$ flux ratio is not that much overestimated anymore in diatom-rich regions (Fig. 11). This result suggests that protactinium has a weaker affinity to biogenic silica than thorium has, though the fractionation is closer to 1 than that of other particle types (Table 2). This result is consistent with Geibert and Usbeck (2004) whose laboratory study shows no definitive affinity of either Th or Pa to biogenic silica. Their average K values actually suggest that thorium has a higher affinity to biogenic silica.

We included lithogenic particles in the model from deposited dust. Since lithogenic particles have a strong relative affinity with $^{230}\mathrm{Th}$ ($K_{\mathrm{Pa,Lith}}/K_{\mathrm{Th,Lith}} = 0.2$) and since they are mostly prevalent in the (northern) Atlantic Ocean, much of the $^{230}\mathrm{Th}$ is scavenged in the Atlantic Ocean. Calcium carbonate $K_{\mathrm{Pa}}/K_{\mathrm{Th}}$ is even smaller (0.024) and is present througout much of the Atlantic but not in the Southern Ocean. This leaves protactinium to be scavenged by biogenic silica in the Southern Ocean when it arrives there through the AMOC. Therefore, even with the smaller-than-conventional K ratio of 0.4 for biogenic silica, the familiar pattern of higher values of Pa/Th in the Southern Ocean compared to most of the rest of the ocean is still reproduced.

7 Conclusion

The purpose of this study is two-fold. Firstly, we wanted to set out a model of $^{231}\mathrm{Pa}$ and $^{230}\mathrm{Th}$, complete with all the necessary particle improvements and additions. This includes an improved underlying particle dynamics from NEMO–PISCES as well as the addition of lithogenic particles. We have succeeded in this, and the model has been presented and implemented such that it can be used for future studies, including for the modelling and validation of ocean circulation in the past.

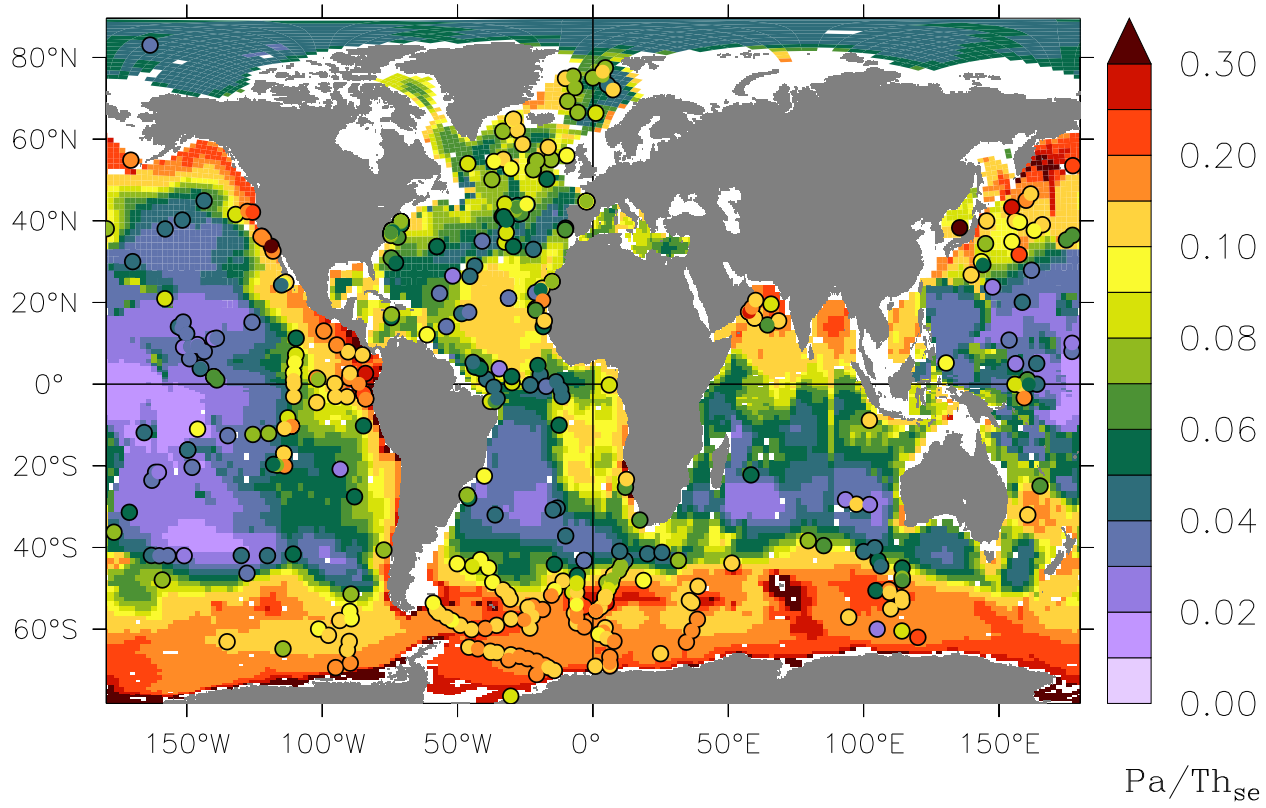

Figure 11. Sedimented ^{231}Pa/^{230}Th ratio when we set $K_{\mathrm{Pa,bSiO_2}}/K_{\mathrm{Th,bSiO_2}} = 0.4$. Top core measurements are presented as discs.

Secondly, this model helps us to study the interplay between particle and water transport that control the ^{231}Pa and ^{230}Th profiles. We have shown that by improving on the particles, we improved the radionuclides, and we have shown to what extent the different particle phases drive the scavenging of ^{231}Pa and ^{230}Th.

Dissolved ^{230}Th and ^{231}Pa concentrations are realistic in intermediate-depth ocean (big improvement compared to Dutay et al. (2009)) but not in the surface: a finite equilibration time between the different radionuclide phases may help. The model can be extended to include this in future versions. It would double the number of adsorption/desorption parameters whose values should be determined through a careful literature and model sensitivity study.

In the deep ocean, the overestimation of ^{230}Th and ^{231}Pa in several regions is likely to be caused, at least partly, by missing nepheloid particles, but also manganese oxides (from hydrothermal vents) may improve the distributions. Additionally, the circulation may be too weak, not freshening AABW fast enough, and hence $[^{230}\mathrm{Th}]_D$ and $[^{231}\mathrm{Pa}]_D$ become too high near the ocean floor.

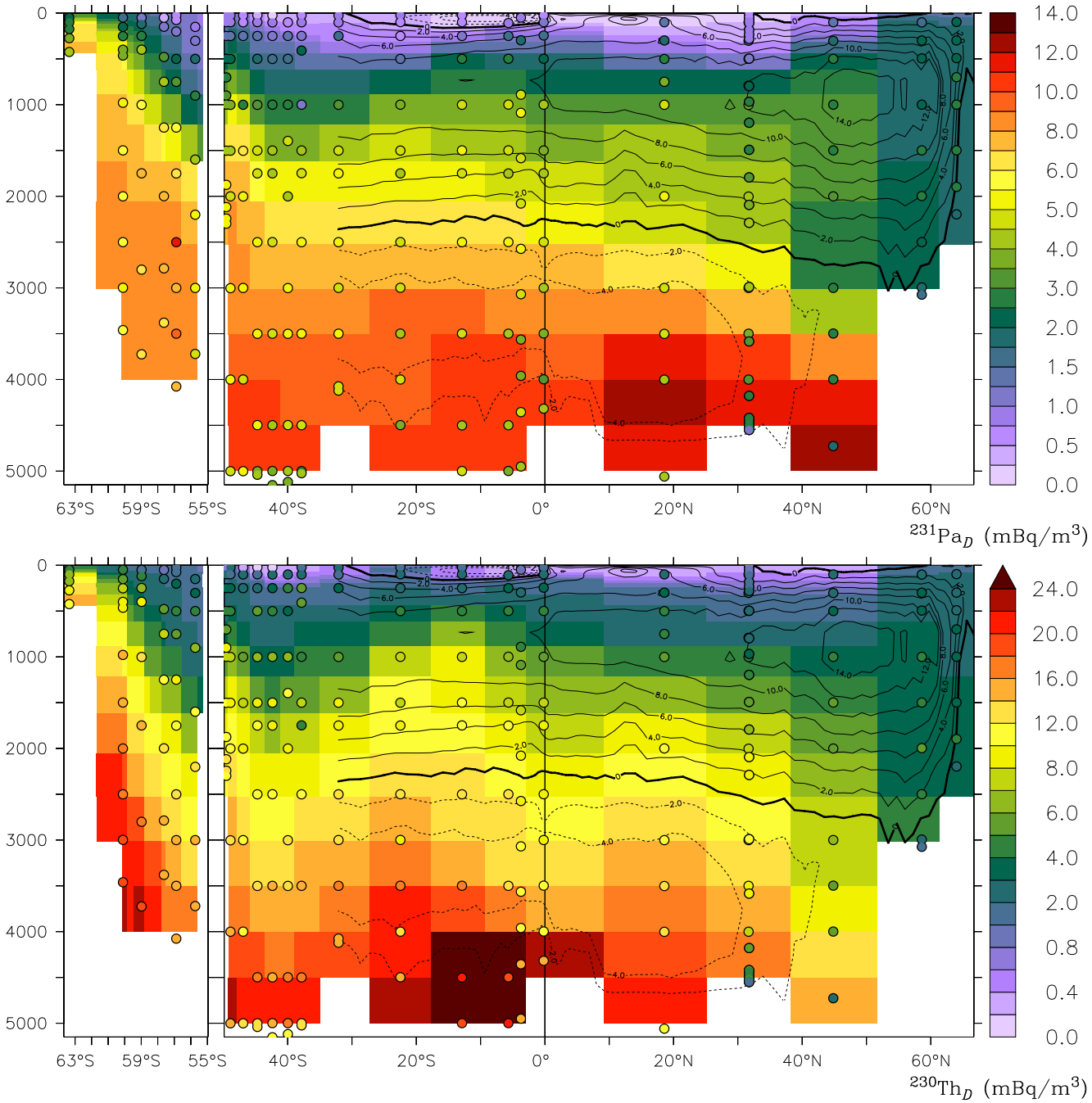

Figure 12. Dissolved protactinium-231 (upper panel), and thorium-230 (lower panel) at the Drake Passage (GIPY5) and West Atlantic (GA02) transects ($\mathrm{mBq\,m^{-3}}$); observations as discs. The Atlantic OSF, in Sv, is superimposed as a contour.

8 Code availability

The mathematical variable names correspond to the Fortran variable as described in Table S1 of the supplementary document. We encourage the reader to use our model, NEMO–ProThorP, to build extended and improved models. We have implemented two particle size classes of adsorbed nuclides, which is the minimum that is needed to produce good results. Instead of introducing a new tracer for every particle type, we only distinguish between "adsorbed onto small particles" and "adsorbed onto big particles", meaning that one is restricted, in this set-up, to include only particles that sink with the two respective settling speeds for scavenging. Whereas this is somewhat restricting, it is computationally efficient, and it restricts the number of degrees of freedom (which is usually a good thing in complex models). NEMO–ProThorP can also be used to set up a non-instant equilibration model (with a k_+ and k_-) that may yield better surface values.

The underlying model, NEMO 3.6 (svn revision 5283), can be downloaded from http://www.nemo-ocean.eu/ (Madec and the NEMO team, 2016) after creating a login. NEMO includes the biogeochemical PISCES model (Aumont et al., 2015). For reproducibility purposes, version 0.1.0 of the radionuclide and lithogenic particles model code can be obtained at https://dx.doi.org/10.5281/zenodo.1009065 (Van Hulten et al., 2017a). However, we plan to make this code available as part of the NEMO model.

The NEMO model is available under the CeCILL free software licence, modelled after the GNU GPL. The lithogenic particles and $^{230}\mathrm{Th}/^{231}\mathrm{Pa}$-specific code is licensed under the same terms, or, at your option, under the GNU General Public License version 3 or higher. The authors do appreciate if, besides the legal adherence to copyleft and attribution, they are informed about the use of the code.

Finally, the most important raw model output files are available at PANGAEA. The Julia scripts used for the statistics are included in the supplementary document. This may be useful to reproduce the results or further inspect the model output.

9 Author contributions

The model and the simulations were designed by MvH, JCD and MRB. MvH implemented the code and performed the simulations. The manuscript was prepared by MvH with close collaboration and major contributions from MRB and JCD.

The authors declare that they have no conflict of interest.

Acknowledgements. We would like to thank Marion Gehlen and Olivier Aumont for the discussions on the calcite parameterisation in PISCES, among other things. The first author is grateful to Jörg Lippold for both the discussion and encouragement that also helped this work.

This study was supported by a Swedish Research Council grant (349-2012-6287) in the framework of the French–Swedish cooperation in the common research training programme in the climate, environment and energy agreement between VR and LSCE, for the project "Particle transport derived from isotope tracers and its impact on ocean biogeochemistry: a GEOTRACES project in the Arctic Ocean". This study was partly supported by the project "Overturning circulation and its implications for the global carbon cycle in coupled models" (ORGANIC, The Research Council of Norway, grant no. 239965).

The authors wish to acknowledge the use of Ferret, a product of NOAA's Pacific Marine Environmental Laboratory. Most of the plots in this paper were created by the Ferret visualisation library ComPlot (Van Hulten, 2017). Finally, the language Julia was used for some of the statistics.

References

Aken, H.M. van: GEOTRACES, the hydrography of the Western Atlantic Ocean, 2011.

Anderson, R.: Chemical tracers of particle transport, Treatise on Geochemistry, 6, 247–273, doi:10.1016/B0-08-043751-6/06111-9, 2003.

Anderson, R., Bacon, M., and Brewer, P.: Removal of ^{230}Th and ^{231}Pa from the open ocean, Earth Planet. Sc. Lett., 62, 7–23, doi:10.1016/0012-821X(83)90067-5, 1983.

Arsouze, T., Dutay, J.-C., Kageyama, M., Lacan, F., Alkama, R., Marti, O., and Jeandel, C.: A modeling sensitivity study of the influence of the Atlantic meridional overturning circulation on neodymium isotopic composition at the Last Glacial Maximum, Clim. of the Past, 4, 191–203, doi:10.5194/cp-4-191-2008, 2008.

Arsouze, T., Dutay, J.-C., Lacan, F., and Jeandel, C.: Reconstructing the Nd oceanic cycle using a coupled dynamical–biogeochemical model, Biogeosci., 6, 2829–2846, doi:10.5194/bg-6-2829-2009, 2009.

Aumont, O., Ethé, C., Tagliabue, A., Bopp, L., and Gehlen, M.: PISCES-v2: an ocean biogeochemical model for carbon and ecosystem studies, Geosci. Model Dev., 8, 2465–2513, doi:10.5194/gmd-8-2465-2015, 2015.

Aumont, O., Hulten, M.M.P. van, Roy-Barman, M., Dutay, J.-C., Éthé, C., and Gehlen, M.: Variable reactivity of particulate organic matter in a global ocean biogeochemical model, Biogeosci., 14, 2321–2341, doi:10.5194/bg-14-2321-2017, 2017.

Ayache, M., Dutay, J.-C., Arsouze, T., Révillon, S., Beuvier, J., and Jeandel, C.: High-resolution neodymium characterization along the Mediterranean margins and modelling of $\varepsilon_{\mathrm{Nd}}$ distribution in the Mediterranean basins, Biogeosci., 13, 5259–5276, doi:10.5194/bg-13-5259-2016, 2016.

Bacon, M. and Anderson, R.: Distribution of Thorium Isotopes Between Dissolved and Particulate Forms in The Deep Sea, J. Geophys. Res., 87, 2045–2056, doi:10.1029/JC087iC03p02045, 1982.

Biastoch, A., Böning, C. W., Getzlaff, J., Molines, J.-M., and Madec, G.: Causes of Interannual–Decadal Variability in the Meridional Overturning Circulation of the Midlatitude North Atlantic Ocean, J. Climate, 21, 6599–6615, doi:10.1175/2008JCLI2404.1, 2008.

Böhm, E., Lippold, J., Gutjahr, M., Frank, M., Blaser, P., Antz, B., Fohlmeister, J., Frank, N., Andersen, M. B., and Deininger, M.: Strong and deep Atlantic meridional overturning circulation during the last glacial cycle, Nature, 517, 73–76, doi:10.1038/nature14059, 2015.

Broecker, W. S., Andree, M., Bonani, G., Wolfli, W., Oeschger, H., Klas, M., Mix, A., and Curry, W.: Preliminary estimates for the radiocarbon age of deep water in the glacial ocean, Paleoceanography, 3, 659–669, doi:10.1029/PA003i006p00659, 1988.

Brun-Cottan, J. C., Auger, R., Lambere, C. E., and Chesselet, R.: Sources and transport of suspended calcites in Pacific Deep Water, J. Mar. Res., 49, 543–564, doi:10.1357/002224091784995837, 1991.

Burckel, P., Waelbroeck, C., Gherardi, J. M., Pichat, S., Arz, H., Lippold, J., Dokken, T., and Thil, F.: Atlantic Ocean circulation changes preceded millennial tropical South America rainfall events during the last glacial, Geophys. Res. Lett., 42, 411–418, doi:10.1002/2014GL062512, 2014GL062512, 2015.

Burckel, P., Waelbroeck, C., Luo, Y., Roche, D. M., Pichat, S., Jaccard, S. L., Gherardi, J., Govin, A., Lippold, J., and Thil, F.: Changes in the geometry and strength of the Atlantic meridional overturning circulation during the last glacial (20–50 ka), Clim. of the Past, 12, 2061–2075, doi:10.5194/cp-12-2061-2016, 2016.

Chase, Z., Anderson, R., Fleisher, M., and Kubik, P.: The influence of particle composition and particle flux on scavenging of Th, Pa and Be in the ocean, Earth Planet. Sc. Lett., 204, 215–229, 2002.

Chuang, C.-Y., Santschi, P. H., Jiang, Y., Ho, Y.-F., Quigg, A., Guo, L., Ayranov, M., and Schumann, D.: Important role of biomolecules from diatoms in the scavenging of particle-reactive radionuclides of thorium, protactinium, lead, polonium, and beryllium in the ocean: A case study with Phaeodactylum tricornutum, Limnol. Oceanogr., 59, 1256–1266, doi:10.4319/lo.2014.59.4.1256, 2014.

Cunningham, S., Kanzow, T., Rayner, D., Baringer, M., Johns, W., Marotzke, J., Longworth, H., Grant, E., Hirschi, J.-M., Beal, L., et al.: Temporal variability of the Atlantic meridional overturning circulation at 26.5° N, Science, 317, 935–938, doi:10.1126/science.1141304, 2007.

Deng, F., Thomas, A. L., Rijkenberg, M. J., and Henderson, G. M.: Controls on seawater ^{231}Pa, ^{230}Th and ^{232}Th concentrations along the flow paths of deep waters in the Southwest Atlantic, Earth Planet. Sc. Lett., 390, 93–102, doi:10.1016/j.epsl.2013.12.038, 2014.

Does, M. van, Korte, L. F., Munday, C. I., Brummer, G.-J. A., and Stuut, J.-B. W.: Particle size traces modern Saharan dust transport and deposition across the equatorial North Atlantic, Atmospheric Chem. Phys. Discuss., 16, 13 697–13 710, doi:10.5194/acp-16-13697-2016, 2016.

Donohue, K. A., Tracey, K. L., Watts, D. R., Chidichimo, M. P., and Chereskin, T. K.: Mean Antarctic Circumpolar Current transport measured in Drake Passage, Geophys. Res. Lett., 43, 11,760–11,767, doi:10.1002/2016GL070319, 2016.

Druffel, E., Williams, P., Bauer, J., and Ertel, J.: Cycling of dissolved and particulate organic matter in the open ocean, J. Geophys. Res., 97, 15 639–15 659, doi:10.1029/92JC01511, http://escholarship.org/uc/item/5pt6w45d, 1992.

Dunk, R., Mills, R., and Jenkins, W.: A reevaluation of the oceanic uranium budget for the Holocene, Chemical Geology, 190, 45–67, doi:10.1016/S0009-2541(02)00110-9, geochemistry of Crustal Fluids-Fluids in the Crust and Chemical Fluxes at the Earth's Surface, 2002.

Dutay, J., Bullister, J., Doney, S., Orr, J., Najjar, R., Caldeira, K., Campin, J., Drange, H., Follows, M., Gao, Y., et al.: Evaluation of ocean model ventilation with CFC-11, Ocean Model., 4, 89–120, doi:10.1016/S1463-5003(01)00013-0, 2002.

Dutay, J., Lacan, F., Roy-Barman, M., and Bopp, L.: Influence of particle size and type on ^{231}Pa and ^{230}Th simulation with a global coupled biogeochemical-ocean general circulation model: A first approach, Geochem. Geophy. Geosy., 10, Q01 011, doi:10.1029/2008GC002291, 2009.

Dutay, J., Tagliabue, A., Kriest, I., and Hulten, M.M.P. van: Modelling the role of marine particle on large scale ^{231}Pa, ^{230}Th, Iron and Aluminium distributions, Prog. Oceanogr., 133, 66–72, doi:10.1016/j.pocean.2015.01.010, 2015.

Gardner, W. D. and Sullivan, L. G.: Benthic storms, Science, 213, 329–331, 1981.

Gardner, W. D., Tucholke, B. E., Richardson, M. J., and Biscaye, P. E.: Benthic storms, nepheloid layers, and linkage with upper ocean dynamics in the western North Atlantic, Mar. Geol., 385, 304–327, doi:10.1016/j.margeo.2016.12.012, 2017.

Gehlen, M., Gangstø, R., Schneider, B., Bopp, L., Aumont, O., and Ethé, C.: The fate of pelagic $CaCO_3$ production in a high CO_2 ocean: a model study, Biogeosci., 4, 505–519, doi:10.5194/bg-4-505-2007, 2007.

Geibert, W. and Usbeck, R.: Adsorption of thorium and protactinium onto different particle types: experimental findings, Geochim. Cosmochim. Ac., 68, 1489–1501, doi:10.1016/j.gca.2003.10.011, 2004.

Gent, P. and McWilliams, J.: Isopycnal mixing in ocean circulation models, J. Phys. Oceanogr., 20, 150–155, doi:10.1175/1520-0485(1990)020<0150:IMIOCM>2.0.CO;2, 1990.

Gent, P., Willebrand, J., McDougall, T., and McWilliams, J.: Parameterizing eddy-induced tracer transports in ocean circulation models, J. Phys. Oceanogr., 25, 463–474, doi:10.1175/1520-0485(1995)025<0463:PEITTI>2.0.CO;2, 1995.

German, C. R., Casciotti, K. A., Dutay, J.-C., Heimbürger, L. E., Jenkins, W. J., Measures, C. I., Mills, R. A., Obata, H., Schlitzer, R., Tagliabue, A., Turner, D. R., and Whitby, H.: Hydrothermal impacts on trace element and isotope ocean biogeochemistry, Phil. Trans. R. Soc. A, 374, doi:10.1098/rsta.2016.0035, part of the special issue *Biological and climatic impacts of ocean trace element chemistry*, 2016.

Gu, S. and Liu, Z.: ^{231}Pa and ^{230}Th in the ocean model of the Community Earth System Model (CESM1.3), Geosci. Model Dev., 10, 4723–4742, doi:10.5194/gmd-10-4723-2017, 2017.

Hauglustaine, D., Hourdin, F., Jourdain, L., Filiberti, M.-A., Walters, S., Lamarque, J.-F., and Holland, E.: Interactive chemistry in the Laboratoire de Météorologie Dynamique general circulation model, J. Geophys. Res.: Atmospheres, 109, D04 314, doi:10.1029/2003JD003957, 2004.

Hayes, C. T., Anderson, R. F., Fleisher, M. Q., Serno, S., Winckler, G., and Gersonde, R.: Quantifying lithogenic inputs to the North Pacific Ocean using the long-lived thorium isotopes, Earth Planet. Sc. Lett., 383, 16–25, doi:10.1016/j.epsl.2013.09.025, 2013.

Hayes, C. T., Anderson, R. F., Fleisher, M. Q., Serno, S., Winckler, G., and Gersonde, R.: Biogeography in ^{231}Pa/^{230}Th ratios and a balanced ^{231}Pa budget for the Pacific Ocean, Earth Planet. Sc. Lett., 391, 307–318, doi:10.1016/j.epsl.2014.02.001, 2014.

Hayes, C. T., Anderson, R. F., Fleisher, M. Q., Huang, K.-F., Robinson, L. F., Lu, Y., Cheng, H., Edwards, R. L., and Moran, S. B.: ^{230}Th and ^{231}Pa on GEOTRACES GA03, the US GEOTRACES North Atlantic transect, and implications for modern and paleoceanographic chemical fluxes, Deep-Sea Res. Pt II, 116, 29–41, doi:10.1016/j.dsr2.2014.07.007, 2015a.

Hayes, C. T., Anderson, R. F., Fleisher, M. Q., Lam, P. J., Ohnemus, D. C., Huang, K.-F., Robinson, L. F., Lu, Y., Cheng, H., Edwards, R. L., and Moran, S. B.: Intensity of Th and Pa scavenging partitioned by particle chemistry in the North Atlantic Ocean, Mar. Chem., 170, 49–60, doi:10.1016/j.marchem.2015.01.006, 2015b.

Heinze, C., Gehlen, M., and Land, C.: On the potential of ^{230}Th, ^{231}Pa, and ^{10}Be for marine rain ratio determinations: A modeling study, Global Biogeochem. Cy., 20, doi:10.1029/2005GB002595, gB2018, 2006.

Henderson, G. M. and Anderson, R. F.: The U-series Toolbox for Paleoceanography, Reviews in Mineralogy and Geochemistry, 52, 493–531, doi:10.2113/0520493, http://rimg.geoscienceworld.org/content/52/1/493.full.pdf+html, 2003.

Henderson, G. M., Heinze, C., Anderson, R. F., and Winguth, A. M.: Global distribution of the ^{230}Th flux to ocean sediments constrained by GCM modelling, Deep-Sea Res. Pt I, 46, 1861–1893, doi:10.1016/S0967-0637(99)00030-8, observational data: http://climotope.earth.ox.ac.uk/data_compilations/holocene_231pa230th_dataset_notes_and_references, 1999.

Honeyman, B. D. and Santschi, P. H.: Metals in aquatic systems, Environmental science & technology, 22, 862–871, 1988.

Honeyman, B. D., Balistrieri, L. S., and Murray, J. W.: Oceanic trace metal scavenging, Deep-Sea Res. Pt A, 35, 227–246, doi:10.1016/0198-0149(88)90038-6, 1988.

Hulten, M.M.P. van: ComPlot: Comparison Plotter to visually evaluate ocean model simulations, The Journal of Open Source Software, 2, doi:10.21105/joss.00368, 2017.

Hulten, M.M.P. van, Sterl, A., Dutay, J.-C., Tagliabue, A., Gehlen, M., Baar, H.J.W. de, and Middag, R.: Aluminium in an ocean general circulation model compared with the West Atlantic GEOTRACES cruises, J. Mar. Syst., 126, 3–23, doi:10.1016/j.jmarsys.2012.05.005, traces and Tracers: Selected papers from the Joint Liège Colloquium on Ocean Dynamics – Bonus-GoodHope – GEOTRACES meeting, 2013.

Hulten, M.M.P. van, Sterl, A., Middag, R., de Baar, H., Gehlen, M., Dutay, J.-C., and Tagliabue, A.: On the effects of circulation, sediment resuspension and biological incorporation by diatoms in an ocean model of aluminium, Biogeosci., 11, 3757–3779, doi:10.5194/bg-11-3757-2014, 2014.

Hulten, M.M.P. van, Dutay, J., and Roy-Barman, M.: Ocean model of Protactinium, Thorium and Particles (ProThorP), doi:10.5281/zenodo.1009064, software package, 2017a.

Hulten, M.M.P. van, Middag, R., Dutay, J.-C., de Baar, H., Roy-Barman, M., Gehlen, M., Tagliabue, A., and Sterl, A.: Manganese in the West Atlantic Ocean in the context of the first global ocean circulation model of manganese, Biogeosci., pp. 1123–1152, doi:10.5194/bg-14-1123-2017, 2017b.

Johnson, G. C.: Quantifying Antarctic Bottom Water and North Atlantic Deep Water volumes, J. Geophys. Res.: Oceans, 113, doi:10.1029/2007JC004477, c05027, 2008.

Kalnay, E., Kanamitsu, M., Kistler, R., Collins, W., Deaven, D., Gandin, L., Iredell, M., Saha, S., White, G., Woollen, J., Zhu, Y., Leetmaa, A., Reynolds, R., Chelliah, M., Ebisuzaki, W., Higgins, W., Janowiak, J., Mo, K. C., Ropelewski, C., Wang, J., Jenne, R., and Joseph, D.: The NCEP/NCAR 40-Year Reanalysis Project, Bull. Amer. Meteor. Soc., 77, 437–471, doi:10.1175/1520-0477(1996)077<0437:TNYRP>2.0.CO;2, 1996.

Keir, R. S.: The dissolution kinetics of biogenic calcium carbonates in seawater, Geochim. Cosmochim. Ac., 44, 241–252, doi:10.1016/0016-7037(80)90135-0, 1980.

Kistler, R., Collins, W., Saha, S., White, G., Woollen, J., Kalnay, E., Chelliah, M., Ebisuzaki, W., Kanamitsu, M., Kousky, V., et al.: The NCEP-NCAR 50-year reanalysis, Bull. Am. Meteorol. Soc., 82, 247–267, doi:10.1175/1520-0477(2001)082<0247:TNNYRM>2.3.CO;2, 2001.

Knippertz, P. and Stuut, J.-B. W.: Mineral Dust, Springer Dordrecht Heidelberg New York London, doi:10.1007/978-94-017-8978-3, 2014.

Kretschmer, S., Geibert, W., van der Loeff, M. M. R., Schnabel, C., Xu, S., and Mollenhauer, G.: Fractionation of ^{230}Th, ^{231}Pa, and ^{10}Be induced by particle size and composition within an opal-rich sediment of the Atlantic Southern Ocean, Geochim. Cosmochim. Ac., 75, 6971–6987, doi:10.1016/j.gca.2011.09.012, 2011.

Ku, T.-L., Knauss, K. G., and Mathieu, G. G.: Uranium in open ocean: concentration and isotopic composition, Deep-Sea Res., 24, 1005–1017, doi:10.1016/0146-6291(77)90571-9, 1977.

Lam, P. J., Doney, S. C., and Bishop, J. K. B.: The dynamic ocean biological pump, Global Biogeochem. Cy., 25, GB3009, doi:10.1029/2010GB003868, 2011.

Lam, P. J., Ohnemus, D. C., and Auro, M. E.: Size-fractionated major particle composition and concentrations from the US GEOTRACES North Atlantic zonal transect, Deep-Sea Res. Pt II, 116, 303–320, doi:10.1016/j.dsr2.2014.11.020, 2015.

Lopez, G. I., Marcantonio, F., Lyle, M., and Lynch-Stieglitz, J.: Dissolved and particulate ^{230}Th–^{232}Th in the Central Equatorial Pacific Ocean: Evidence for far-field transport of the East Pacific Rise hydrothermal plume, Earth Planet. Sc. Lett., 431, 87–95, doi:10.1016/j.epsl.2015.09.019, 2015.

Luo, Y., Francois, R., and Allen, S. E.: Sediment ^{231}Pa/^{230}Th as a recorder of the rate of the Atlantic meridional overturning circulation: insights from a 2-D model, Ocean Sci., 6, 381–400, doi:10.5194/os-6-381-2010, 2010.

Madec, G.: NEMO ocean engine, Note du Pole de Modélisation, Institut Pierre-Simon Laplace, 2008.

Madec, G. and Imbard, M.: A global ocean mesh to overcome the North Pole singularity, Clim. Dyn., 12, 381–388, doi:10.1007/BF00211684, 1996.

Madec, G. and the NEMO team: NEMO ocean engine, Note du Pole de Modélisation, Institut Pierre-Simon Laplace, 2016.

Marchal, O., François, R., Stocker, T., and Joos, F.: Ocean thermohaline circulation and sedimentary ^{231}Pa/^{230}Th ratio, Paleoceanography, 15, 625–641, doi:10.1029/2000PA000496, 2000.

Marchal, O., François, R., and Scholten, J.: Contribution of ^{230}Th measurements to the estimation of the abyssal circulation, Deep-Sea Res. Pt I, 54, 557–585, doi:10.1016/j.dsr.2007.01.002, there is an erratum (for figure labels), 2007.

Mawji, E., Schlitzer, R., Dodas, E. M., Abadie, C., Abouchami, W., Anderson, R. F., Baars, O., Bakker, K., Baskaran, M., Bates, N. R., Bluhm, K., Bowie, A., Bown, J., Boye, M., Boyle, E. A., Branellec, P., Bruland, K. W., Brzezinski, M. A., Bucciarelli, E., Buesseler, K., Butler, E., Cai, P., Cardinal, D., Casciotti, K., Chaves, J., Cheng, H., Chever, F., Church, T. M., Colman, A. S., Conway, T. M., Croot, P. L., Cutter, G. A., de Baar, H. J., de Souza, G. F., Dehairs, F., Deng, F., Dieu, H. T., Dulaquais, G., Echegoyen-Sanz, Y., Edwards, R. L., Fahrbach, E., Fitzsimmons, J., Fleisher, M., Frank, M., Friedrich, J., Fripiat, F., Galer, S. J., Gamo, T., Solsona, E. G., Gerringa, L. J., Godoy, J. M., Gonzalez, S., Grossteffan, E., Hatta, M., Hayes, C. T., Heller, M. I., Henderson, G., Huang, K.-F., Jeandel, C., Jenkins, W. J., John, S., Kenna, T. C., Klunder, M., Kretschmer, S., Kumamoto, Y., Laan, P., Labatut, M., Lacan, F., Lam, P. J., Lannuzel, D., le Moigne, F., Lechtenfeld, O. J., Lohan, M. C., Lu, Y., Masqué, P., McClain, C. R., Measures, C., Middag, R., Moffett, J., Navidad, A., Nishioka, J., Noble, A., Obata, H., Ohnemus, D. C., Owens, S., Planchon, F., Pradoux, C., Puigcorbé, V., Quay, P., Radic, A., Rehkämper, M., Remenyi, T., Rijkenberg, M. J., Rintoul, S., Robinson, L. F., Roeske, T., Rosenberg, M., Rutgers van der Loeff, M., Ryabenko, E., Saito, M. A., Roshan, S., Salt, L., Sarthou, G., Schauer, U., Scott, P., Sedwick, P. N., Sha, L., Shiller, A. M., Sigman, D. M., Smethie, W., Smith, G. J., Sohrin, Y., Speich, S., Stichel, T., Stutsman, J., Swift, J. H., Tagliabue, A., Thomas, A., Tsunogai, U., Twining, B. S., van Aken, H. M., van Heuven, S., van Ooijen, J., van Weerlee, E., Venchiarutti, C., Voelker, A. H., Wake, B., Warner, M. J., Woodward, E. M. S., Wu, J., Wyatt, N., Yoshikawa, H., Zheng, X.-Y., Xue, Z., Zieringer, M., and Zimmer, L. A.: The GEOTRACES Intermediate Data Product 2014, Mar. Chem., 177, 1–8, doi:10.1016/j.marchem.2015.04.005, the complete dataset can be downloaded from http://www.geotraces.org/dp/idp2014., 2015.

Mouchet, A.: The Ocean Bomb Radiocarbon Inventory Revisited, Radiocarbon, 55, 1580–1594, doi:10.1017/S0033822200048505, 2013.

Murray, R.: Explicit generation of orthogonal grids for ocean models, J. Comput. Phys., 126, 251–273, doi:10.1006/jcph.1996.0136, 1996.

Owens, S., Buesseler, K., and Sims, K.: Re-evaluating the ^{238}U-salinity relationship in seawater: Implications for the ^{238}U–^{234}Th disequilibrium method, Mar. Chem., 127, 31–39, doi:10.1016/j.marchem.2011.07.005, 2011.

Pavia, F., Anderson, R., Vivancos, S., Fleisher, M., Lam, P., Lu, Y., Cheng, H., Zhang, P., and Edwards, R. L.: Intense hydrothermal scavenging of ^{230}Th and ^{231}Pa in the deep Southeast Pacific, Mar. Chem., doi:10.1016/j.marchem.2017.08.003, 2017.

Piotrowski, A. M., Goldstein, S. L., Hemming, S. R., and Fairbanks, R. G.: Temporal Relationships of Carbon Cycling and Ocean Circulation at Glacial Boundaries, Science, 307, 1933–1938, doi:10.1126/science.1104883, 2005.

Rayner, D., Hirschi, J.-M., Kanzow, T., Johns, W., Wright, P., Frajka-Williams, E., Bryden, H., Meinen, C., Baringer, M., Marotzke, J., et al.: Monitoring the Atlantic meridional overturning circulation, Deep-Sea Res. Pt II, 58, 1744–1753, doi:10.1016/j.dsr2.2010.10.056, 2011.

Rempfer, J., Stocker, T. F., Joos, F., Lippold, J., and Jaccard, S. L.: New insights into cycling of ^{231}Pa and ^{230}Th in the Atlantic Ocean, Earth Planet. Sc. Lett., 468, 27–37, doi:10.1016/j.epsl.2017.03.027, units of ^{231}Pa and ^{230}Th activities/concentrations are dpm/m^3, 2017.

Rosenthal, Y., Boyle, E. A., and Labeyrie, L.: Last Glacial Maximum paleochemistry and deepwater circulation in the Southern Ocean: Evidence from foraminiferal cadmium, Paleoceanography, 12, 787–796, doi:10.1029/97PA02508, 1997.

Roy-Barman, M.: Modelling the effect of boundary scavenging on Thorium and Protactinium profiles in the ocean, Biogeosci., 6, 3091–3107, doi:10.5194/bg-6-3091-2009, 2009.

Roy-Barman, M., Chen, J., and Wasserburg, G.: ^{230}Th–^{232}Th systematics in the central Pacific Ocean: The sources and the fates of thorium, Earth Planet. Sc. Lett., 139, 351–363, doi:10.1016/0012-821X(96)00017-9, 1996.

Rutgers van der Loeff, M., Venchiarutti, C., Stimac, I., Ooijen, Jan van, Huhn, O., Rohardt, G., and Strass, V.: Meridional circulation across the Antarctic Circumpolar Current serves as a double ^{231}Pa and ^{230}Th trap, Earth Planet. Sc. Lett., 455, 73–84, doi:10.1016/j.epsl.2016.07.027, 2016.

Siddall, M., Henderson, G., Edwards, N., Frank, M., Müller, S., Stocker, T., and Joos, F.: ^{231}Pa/^{230}Th fractionation by ocean transport, biogenic particle flux and particle type, Earth Planet. Sc. Lett., 237, 135–155, doi:10.1016/j.epsl.2005.05.031, 2005.

Siddall, M., Stocker, T. F., Henderson, G. M., Joos, F., Frank, M., Edwards, N. R., Ritz, S. P., and Müller, S. A.: Modeling the relationship between ^{231}Pa/^{230}Th distribution in North Atlantic sediment and Atlantic meridional overturning circulation, Paleoceanography, 22, doi:10.1029/2006PA001358, 2007.

Sinha, B., Smeed, D., McCarthy, G., Moat, B., Josey, S., Hirschi, J.-M., Frajka-Williams, E., Blaker, A., Rayner, D., and Madec, G.: The accuracy of estimates of the overturning circulation from basin-wide mooring arrays, Prog. Oceanogr., 160, 101–123, doi:10.1016/j.pocean.2017.12.001, 2018.

Subhas, A. V., Rollins, N. E., Berelson, W. M., Dong, S., Erez, J., and Adkins, J. F.: A novel determination of calcite dissolution kinetics in seawater, Geochim. Cosmochim. Ac., 170, 51–68, doi:10.1016/j.gca.2015.08.011, 2015.

Tagliabue, A., Bopp, L., Roche, D., Bouttes, N., Dutay, J., Alkama, R., Kageyama, M., Michel, E., Paillard, D., et al.: Quantifying the roles of ocean circulation and biogeochemistry in governing ocean carbon-13 and atmospheric carbon dioxide at the last glacial maximum, Clim. of the Past, 5, 695–706, 2009.

Tagliabue, A., Bopp, L., Dutay, J.-C., Bowie, A., Chever, F., Jean-Baptiste, P., Bucciarelli, E., Lannuzel, D., Remenyi, T., Sarthou, G., Aumont, O., Gehlen, M., and Jeandel, C.: Hydrothermal contribution to the oceanic dissolved iron inventory, Nat. Geosci., 3, 252–256, doi:10.1038/NGEO818, 2010.

Talley, L., Reid, J., and Robbins, P.: Data-based meridional overturning streamfunctions for the global ocean, J. Climate, 16, 3213–3226, doi:10.1175/1520-0442(2003)016<3213:DMOSFT>2.0.CO;2, 2003.

Timmermann, R., Goosse, H., Madec, G., Fichefet, T., Ethé, C., and Dulière, V.: On the representation of high latitude processes in the ORCA-LIM global coupled sea ice–ocean model, Ocean Model., 8, 175–201, doi:10.1016/j.ocemod.2003.12.009, 2005.

Venchiarutti, C., Rutgers van der Loeff, M., and Stimac, I.: Scavenging of ^{231}Pa and thorium isotopes based on dissolved and size-fractionated particulate distributions at Drake Passage (ANTXXIV-3), Deep-Sea Res. Pt II, 58, 2767–2784, doi:10.1016/j.dsr2.2010.10.040, physics, Carbon Dioxide, Trace Elements and Isotopes in the Southern Ocean: The Polarstern Expeditions ANT XXIV-3 (2008) and ANT XXIII/3 (2006), 2011.

Yu, E.-F., Francois, R., and Bacon, M. P.: Similar rates of modern and last-glacial ocean thermohaline circulation inferred, Nature, 379, 22, doi:10.1038/379689a0, 1996.